Electrostatic tether plasma brake

ESA CleanSat Building Block 15 (BB15) final report

Pekka Janhunen, Petri Toivanen & Jouni Envall

January 18, 2017

Finnish Meteorological Institute

AD-citable and LSI version of the document

Table of contents

Cover page **1**

List of acronyms **4**

Executive summary **5**

1 Introduction: study objectives **8**

2 Applicable & reference documents **10**
2.1 Applicable documents 10
2.2 Reference documents 10

3 Requirements during the BB design **12**
3.1 LSI requirements understanding and harmonisation 12
3.1.1 Airbus Defence and Space requirements 12
3.1.2 OHB requirements 13
3.1.3 Harmonised requirements 14
3.2 Consolidated Building Block requirements specification and statement of compliance 19

4 Design work logic **20**
4.1 Cold gas thruster deployed gravity-stabilised tether 21
4.2 Spin deployment option 21
4.3 Spring deployed gravity-stabilised tether 22

5 Design description **23**
5.1 Functional analysis and main problem areas identification 23
5.2 Design concept architecture 25
5.3 Design concept interfaces 26
5.3.1 Mechanical interface 26
5.3.2 Electrical interface 27
5.3.3 Thermal interface 28
5.4 Design concept performance and budgets 28
5.5 System level impacts 29
5.6 Inputs for demisability analyses at system level 30

6 Design justification **30**
6.1 Solutions trade-off 30
6.1.1 Material selection 30
6.1.2 Device geometry selection 31
6.1.3 Minimum tether tension in deployment phase 32
6.1.4 To use a battery or not 33
6.1.5 The mass of RU2 34
6.2 Analyses, simulations and test results 34
6.2.1 Conductivity 34
6.2.2 Sputtering 34

6.2.3 ATOX tolerance . . . 37
6.2.4 Mechanical strength . . . 37
6.2.5 Low-temperature ductility . . . 38
6.2.6 Material cost . . . 38
6.2.7 Formula for predicting the thrust . . . 38
6.2.8 Plasma conditions in orbit . . . 40
6.2.9 Ion current collection . . . 41
6.2.10 Balancing electron current collection . . . 44
6.2.10.1 Parker-Murphy theory . . . 45
6.2.11 Deorbiting time . . . 47
6.2.12 Failure probability of deorbiting . . . 47
6.2.12.1 Other failure modes besides tether breakage . . . 49
6.2.12.2 Risk to active satellites . . . 50
6.2.13 Simulation of tether dynamics . . . 51
6.2.14 Deployment simulation . . . 60

7 Development plan **64**
7.1 Development roadmap . . . 64
7.1.1 Foreseen activities . . . 64
7.1.2 Initial TRL . . . 65
7.1.3 Final TRL . . . 65
7.2 Identification of risks . . . 65
7.3 Assembly, integration and test . . . 65
7.4 Costs . . . 66

8 Conclusions **66**

A Annex 1: Facilities and tools used for the study **67**
A.1 Code used for calculating deorbit times in Table 17 . . . 67

List of acronyms

ADS	The Airbus Defence and Space company
ATOX	Atomic oxygen
BB	Building block
BCC	Body-centred cubic crystal structure
BOL	Beginning of life
BU	Base unit
CAD	Computer-aided design
CDF	Concurrent Design Facility (of ESTEC)
CDF1	First project meeting held at Concurrent Design Facility
CG	Cold gas (thruster)
Delta-V	Velocity change
DRAMA	ESA's Debris Risk Assessment and Mitigation Analysis software tool
EOL	End of life
EPS	Electric power system
EST	Electrostatic tether
ESTEC	European Space research and TEchnology Centre
FCC	Face-centred cubic crystal structure
F-RAM	Ferroelectric random access memory
HCP	Hexagonal close-packed crystal structure
HV	High voltage
ITO	Indium tin oxide
LEO	Low Earth orbit
LSI	Large system integrator company/companies (Airbus, OHB, Thales-Alenia)
OHB	The OHB company
PCB	Printed circuit board
R&D	Research and development
RU	Remote unit
RU1,RU2	Remote unit 1 and 2
S/C	Spacecraft
SDM	Space debris mitigation
SS	Stainless steel
SSO	Sun-synchronous orbit
TBC	To be confirmed
TBD	To be decided
TC	Telecommand
TETR	Tetragonal crystal structure
TRL	Technical readiness level
U	One cubesat unit (cube whose side length is about 10 cm)
WP	Work package
/w	with

Executive summary

The electrostatic tether plasma brake is a new concept for deorbiting a LEO satellite. The method uses a thin charged tether for tapping momentum from the plasma ram flow by Coulomb drag. The device module is lightweight (2 kg) and low-cost (50 k€ recurrent) and it can deorbit a 400 kg satellite from 850 km or a 100 kg satellite from 1200 km in about 6 years. If one uses two modules, the masses are doubled to 800 kg and 200 kg, respectively. Comprehensive dynamical simulations show that the tether system oscillates in orbit at a certain amplitude during deployment and deorbiting, but remains dynamically long-term stable.

The geometry and operating principle of the plasma brake module is shown in Fig. 1. The module consists of a base unit (BU) which is bolted to the satellite's bottom or top, and two remote units (RU1 and RU2, Fig. 1a).

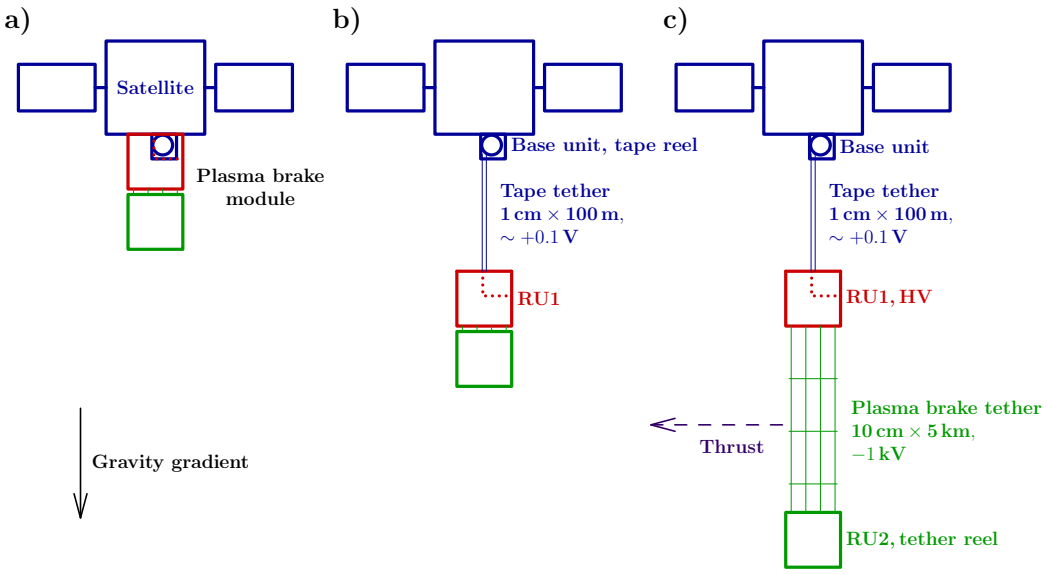

Figure 1: Schematic of the device in deployed state when deployment occurs downwards: a) stowed state, b) tape tether deployed, c) also electrostatic tether deployed.

The deployment occurs in two phases. First the RU1+RU2 combination is ejected from the BU by a spring, which also opens a 100 m long 1 cm wide and 12.6 μm thin aluminium coated kapton tape tether from a BU reel (Fig. 1b). To avoid the bounceback phenomenon, the tape tether is passively braked near the end. In the second phase the RU2 is separated from RU1, and the 5 km long maintether is deployed (Fig. 1c). The deployment occurs with the help of the gravity gradient tension: the 100 m long tape tether provides sufficient separation from the centre of mass of the system to give a large enough gravity gradient force exerted on RU2 to enable reliable deployment of the maintether.

The maintether is made of five interconnected 35 μm diameter aluminium wires, is 8 cm wide and weighs 65 grams. The redundant structure is necessary for the tether to survive inevitable single wire cuttings by micrometeoroid and debris particle impacts.

After deployment is complete, a high-voltage source (1 kV) with low power consumption (2 W) is turned on in RU1. The voltage source forces the maintether to become negative with respect to the aluminium coated tape tether. The tape tether then also

acts as an electron collecting surface and it settles at about the ambient plasma potential. As a result, the maintether gets biased at −1 kV with respect to the plasma. The high-voltage source is powered permanently except when the satellite is in eclipse. No energy storage devices are needed. This keeps costs down and enables long shelf life and orbital life without servicing.

From the point of view of the host satellite, the plasma brake module is a passive device. After deployment, the module accomplishes deorbiting autonomously with no help from the satellite. The RU1 and RU2 are covered by solar panels to generate the electric power needed for the high-voltage source. Therefore the satellite can passivate itself electrically when deployment is complete.

Models of the BU, RU1 and RU2 are shown in Fig. 2 as CAD drawings. RU1 and RU2 are 1-U cubesat sized.

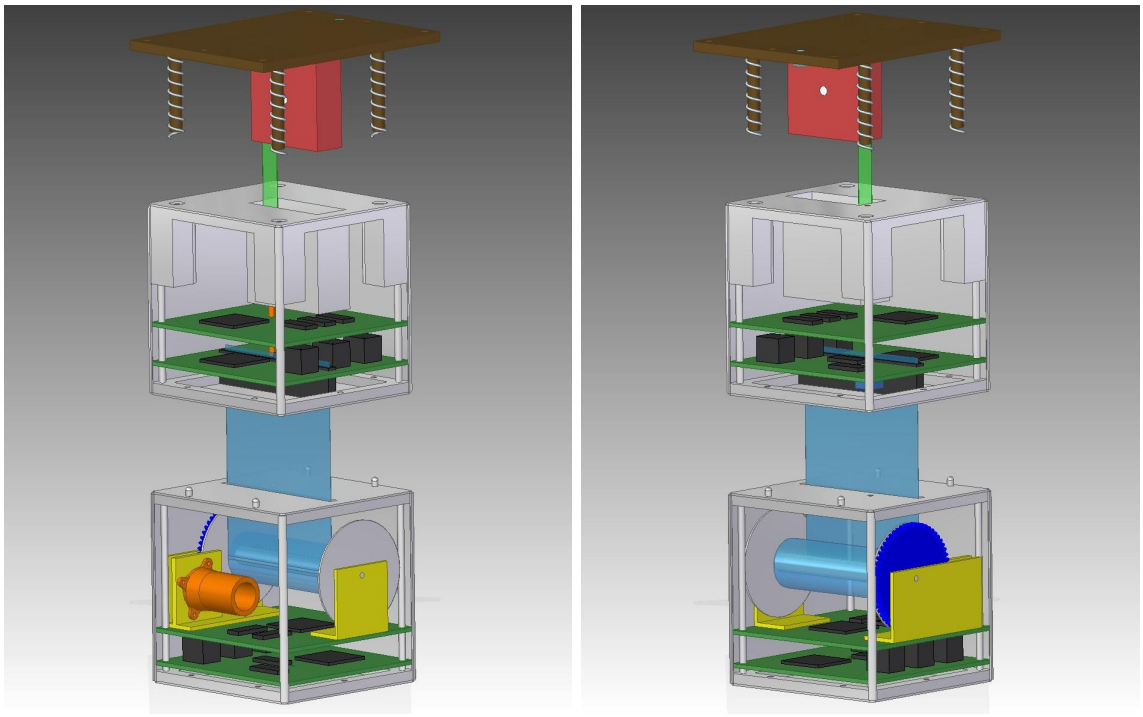

Figure 2: Opened plasma brake module viewed from two directions. Units from top to bottom: BU, RU1, RU2.

The satellite may carry either one or two modules. If two modules are used, one tether is deployed upward and the other one downward. The tethers are tensioned in both directions by the gravity gradient. Using two modules doubles the braking force and increases reliability by providing redundancy.

As the tether wire is thin, the tether poses no threat to other satellites. If the tether breaks, the remaining piece of the tether and a spare high-voltage source in RU2 guarantee that the detached RU2 deorbits itself quickly so that no debris is left behind. After tether breakage, also deorbiting of the satellite continues by the remaining tether piece, although at a slower pace. If two modules are used, then the reliability is even higher.

Presently we have three methods for tether production. One method is an ultrasonic bonding method at TRL 4 which was developed in an earlier EU FP7 project. The

method works, but is somewhat inherently expensive to apply. A newer inexpensive production method is at TRL 3, but the materials that it works with are not quite optimal for the LEO environment. Finally there is a new inexpensive method at TRL 1 which works also with optimal LEO tether materials.

We performed long-term (up to ten days) dynamical simulations of the tether system with a very accurate 8th order first-principles numerical code developed earlier in an EU FP7 project. The code includes tether elasticity, material damping, thermal contraction and the gravitational and plasma forces acting on the tether. The satellite and the remote units are modelled as rigid bodies of the true size. Also full orbital dynamics is self-consistently included in the same simulation. According to the simulation, the tether oscillates at a certain amplitude but is dynamically stable, including flying through eclipse. We also simulated tether deployment and it is also dynamically stable.

The Finnish Aalto-1 cubesat carries an experiment which will attempt to measure the plasma brake Coulomb drag effect in LEO. Aalto-1 will be launched in Q1/2017 with the SHERPA launch of Falcon-9.

The cornerstones of the roadmap activities are development of the inexpensive tether production and in-orbit demonstration of the module. The in-orbit demonstration mission can be either a dedicated self-contained 3-U cubesat or the module can be hosted on a normal LEO satellite.

1 Introduction: study objectives

The Coulomb drag plasma brake [2, 3, 6] uses a long and thin negatively charged tether to tap momentum from the ionospheric plasma. The satellite moves through approximately stationary ionospheric plasma by virtue of its orbital motion, and if one charges the tether up negatively, enhanced Coulomb friction between the tether and the ram flow of the plasma develops. The Coulomb friction slowly brakes the satellite's orbital motion. The benefits of the system include low mass, low power consumption and safety to other space assets (6.2.12.2). The tether is made of wires so thin ($\sim 25\,\mu$m) that even in the case of impact the scratch produced by it is similar to the scratches that are produced all the time in satellites by the existing micrometeoroid and space debris fluxes. Orbital testing of Coulomb drag propulsion will be attempted by the Aalto-1 cubesat [8] which is currently waiting for launch onboard Space-X Falcon-9 SHERPA in Q1/2017.

The objective of this study is to design a modular plasma brake device that can deorbit satellites up to several hundred kilogram mass, by using technical requirements set by LSIs and ESA. Writing a roadmap for developing the device to TRL 7 is also part of this study.

There are several material and environmental parameters that affect the optimisation of the plasma brake design. These include material conductivity, mechanical strength, tolerance of at least $-100..+100$°C temperature range (including not becoming brittle at low temperature), resistance of ion sputtering and atomic oxygen (ATOX) and magnetic properties. Furthermore the material should also be safe to handle, inexpensive and suitable for manufacturing of multi-wire tether. Many of the parameters are interrelated. For example, a strong and well-conducting material allows a longer tether that brings down the satellite faster which reduces the issues of sputtering and ATOX. As another example, if the material's conductivity is rather poor, its strength does not help much because the conductivity anyway limits the usable tether length. The same holds in the other direction as well. For performance of the system, ionospheric plasma density and its distribution in altitude, latitude and longitude as well as solar cycle dependence play a role. Also the oxygen to hydrogen ion ratio is relevant: heavier oxygen ions speed up deorbiting, but they also increase sputtering.

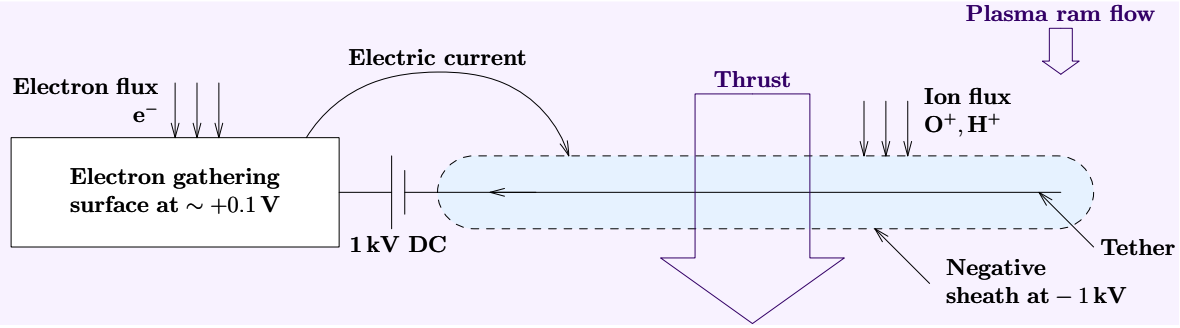

Figure 3: General principle and current closure of the electrostatic plasma brake.

Figure 3 shows the electrostatic operating principle of the plasma brake. The device needs an electron collecting surface which can be either the satellite body or (as in our baseline case) a metal-coated plastic tape tether. The thrust is due to scattering of

ram flow ions by the negative potential structure – it is *not* due to the current flowing in the tether as is the case in the traditional electrodynamic tether. The plasma brake tether is made as thin as possible in order to gather as low current as possible in order to minimise the power consumption of the device. Because the tether is thin, the mass of the device is low and the tether is safe to other space assets even in the event of unwanted collision (6.2.12.2).

The electrostatic plasma brake can only be used to take down satellites and not for increasing the orbital altitude. However, the braking force could be controlled by controlling the voltage and one could use this capability for example for spreading out the orbits of a satellite swarm to avoid the use of launch vehicle propulsion for that. In the present study our aim is plain deorbiting of satellites and the device we will consider does not need a control capability.

Figure 4 shows schematically the gravity-stabilised plasma brake in action. The figure shows the Aalto-1 3-U cubesat, but in the present study we will find out that a similar gravity-stabilised brake is applicable for up to 800 kg mass satellites. Also, a second upward deployed tether can be added to double the thrust because the gravity gradient produces tether tension nearly symmetrically upward and downward.

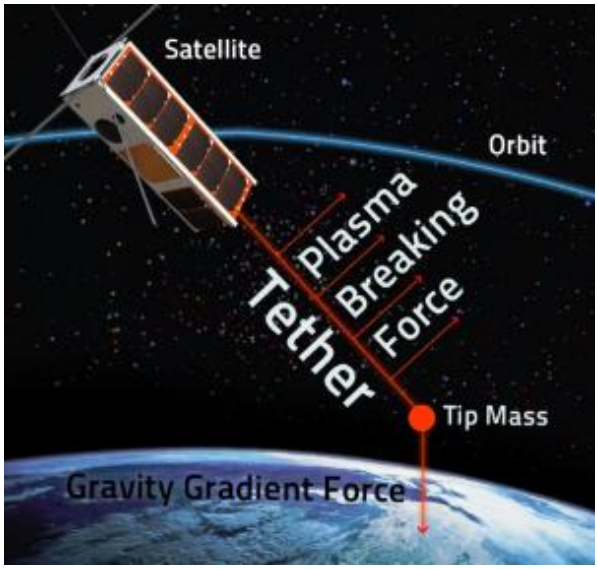

Figure 4: Artist's view of the single-tether gravity-stabilised plasma brake. The inclination of the tether due to the Coulomb drag is drawn exaggerated.

2 Applicable & reference documents

2.1 Applicable documents

[AD1] CleanSat: Technology assessment and concurrent engineering in support of LEO platform evolutions, ESA-TEC-SC-SOW-2015-001, European Space Agency, 2015.

[AD2] Margin philosophy for science assessment studies, SRE-PA/2011.097/, Issue 2, rev. 0, European Space Agency, 2014.

2.2 Reference documents

[1] Janhunen, P. and A. Sandroos, Simulation study of solar wind push on a charged wire: basis of solar wind electric sail propulsion, Ann. Geophys., 25, 755–767, 2007.

[2] Janhunen, P., On the feasibility of a negative polarity electric sail, Ann. Geophys., 27, 1439–1447, 2009.

[3] Janhunen, P., Electrostatic plasma brake for deorbiting a satellite, J. Prop. Power, 26, 370–372, 2010.

[4] Janhunen, P., Description of E-sail dynamic simulator codes, ESAIL FP7 project deliverable D51.1, Finnish Meteorological Institute, 2013, `http://www.electric-sailing.fi/fp7/docs/D511.pdf` .

[5] Janhunen, P., Report of performed runs, ESAIL FP7 project deliverable D51.2, Finnish Meteorological Institute, 2013, `http://www.electric-sailing.fi/fp7/docs/D51.2.pdf` .

[6] Janhunen, P., Simulation study of the plasma-brake effect, Ann. Geophys., 32, 1207–1216, 2014.

[7] Janhunen, P. and P. Toivanen, Safety criteria for flying E-sail through solar eclipse, Acta Astronaut., 114, 1–5, 2015.

[8] Kestilä, A., T. Tikka, P. Peitso, J. Rantanen, A Näsilä, K. Nordling, H. Saari, R. Vainio, P. Janhunen, J. Praks and M. Hallikainen, Aalto-1 nanosatellite – technical description and mission objectives, Geosci. Instrum. Method. Data Syst., 2, 121–130, 2013.

[9] Laframboise, J.G. and L.J. Sonmor, Current collection in magnetoplasma, in "Current Collection from Space Plasmas", NASA CP–3089, pp. 13–49, edited by N. Singh, K.H. Wright, Jr. and N.H. Stone, NASA Marshall Space Flight Center, 1990.

[10] Parker, L.W. and B.L. Murphy, Potential buildup on an electron-emitting ionospheric satellite, J. Geophys. Res., 72, 1631–1636, 1967.

[11] Rosta, R. and T. Wippermann, Tether reeling test report, ESAIL project deliverable D3.1.4, `http://www.electric-sailing.fi/fp7/docs/D314.pdf`.

[12] Rubinstein, J. and J.G. Laframboise, Theory of a spherical probe in collisionless magnetoplasma, Phys. Fluids, 25, 1174–1182, 1982.

[13] Seppänen, H., Kiprich, S., Kurppa, R., Janhunen, P. and Hæggström, E., Wire-to-wire bonding of um-diameter aluminum wires for the Electric Solar Wind Sail, Microelectronic Engineering, 88, 3267–3269, 2011.

[14] Seppänen, H., T. Rauhala, S. Kiprich, J. Ukkonen, M. Simonsson, R. Kurppa, P. Janhunen and E. Hæggström, One kilometer (1 km) electric solar wind sail tether produced automatically, Rev. Sci. Instrum., 84, 095102, 2013.

[15] Timmerhaus, K.D. and T.M. Flynn, Cryogenic process engineering, p. 44, Int. Cryogenic Monograph Series, ISBN 978-1-4684-8758-9, 1989.

[16] Technical University of Vienna sputter yield calculator, `http://www.iap.tuwien.ac.at/www/surface/sputteryield`.

[17] International Reference Ionosphere 2007 model, `http://omniweb.gsfc.nasa.gov/vitmo/iri_vitmo.html`.

3 Requirements during the BB design

In this section the LSI requirements by Airbus and OHB are listed together with the harmonised requirements which were defined at the CDF1 meeting. After that we consider in tabular form the compliance of the proposed design to the harmonised requirements.

3.1 LSI requirements understanding and harmonisation

3.1.1 Airbus Defence and Space requirements

The original Airbus Defence and Space (ADS) requirements are the following. The requirement itself is written in *italics*, any text following it is additional explanation.

BB15-ADS001 Mass. *The device mass shall be inferior to 5 kg (TBC).* For a satellite class of 500 kg dry in order to perform a delta-V of 50 m/s (for de-orbiting) it would be necessary to add 10 kg of chemical propellant (i.e. 10 liters).

BB15-ADS002 Volume – Dimensions. *The volume of the undeployed device shall not exceeed 10 liters (TBC).*

BB15-ADS003 Functional. *The device shall be triggering through ground TC.*

BB15-ADS004 Functional. *The device deployment shall be compatible with the following S/C dynamic conditions: angular rate conditons* $< 2°/s$ *about any spacecraft axis.*

BB15-ADS005 Functional. *The deployed device shall not require any resource (e.g. power) from the spacecraft during the disposal phase.* During the disposal phase, the satellite will be switched off.

BB15-ADS006 Performance. *The device performances shall be ensured for orbits up to 850 km altitude, with any orbit inclination.*

BB15-ADS007 Performance. *Passive device once deployed (no power supplied by the platform during the disposal phase).* Tether only (if necessary power supplied by the device itself).

BB15-ADS008 Performance. *Once deployed, the device shall ensure a satellite uncontrolled re-entry in less than 25 years.* Maximum Altitude 850 km. 2 application cases: i) S/C mass of 200 kg and a ballistic coefficient of 130 kg/m^2, ii) S/C mass of 500 kg and a ballistic coefficient of 130 kg/m^2.

BB15-ADS009 Reliability. *The reliability of the device deployment/operations shall be superior to 95 % (TBC).* There will be in a near future a global spec relative to the probability of achievement of EOL operations.

BB15-ADS010 Safety. *There shall be no spurious triggering during nominal in-orbit operations.* The mission shall not be jeopardised by an unwanted deployment of the device (safety=100 %).

BB15-ADS011 Lifetime On-Ground. *The device design shall be compatible of 10 years (TBC) ground storage, without need for complimentary re-acceptance testing at the end of the storage period.*

BB15-ADS012 Lifetime In-Orbit. *The device performance and reliability figures shall be guaranteed during the following mission operation lifetime: 10 years for LEO missions.*

BB15-ADS013 Environment – Radiation. *The device shall ensure the expected performance under the radiation conditions observed during the operational lifetime*

and the disposal phase.

BB15-ADS014 Environment – ATOX. *The deployed device shall be compatible with atomic oxygen environment in the altitude range from 200 to 850 km.*

BB15-ADS015 Demisability. *The device shall totally demise when exposed to the thermal flux from an altitude of 78 km.* We do not want the device to increase the casualty area on ground (an increase might put into question the uncontrolled re-entry).

BB-ADS016 Cost. *The device cost shall not exceeed 50 k (TBC).* This cost has to be compared to the cost of additional propellant (e.g. hydrazine or xenon) and the extra cost due to a larger tank.

We drop BB15-ADS007 because it expressed the same thing as BB15-ADS005.

3.1.2 OHB requirements

The original OHB requirements are the following.

BB15-OHB-01 Subsystem. *The EST device shall be a separate "bolt-on" subsystem with clearly defined interfaces to the spacecraft.* This necessitates the set-up of a subsystem ICD by the contractor.

BB15-OHB-02 States and Modes. *The EST shall have at least two discrete states, a stowed and a deployed state, and a deployment mode which sets the device from the stowed to the deployed state.* Further states and modes may exist. Please specify clearly.

BB15-OHB-03 Lifetime. *In stowed state the device shall be mounted on any outside panel of a LEO satellite during launch and operations of up to 5 years (threshold), 10 years (goal).* Demonstrate that the device is able to cope with any environmental conditions encountered during launch and LEO operations in any attitude (launch loads/hot case/cold case).

BB15-OHB-04 Lifetime. *In deployed state the device shall survive until re-entry in orbital altitudes between 250 km and 2000 km.* Demonstrate that the device is able to cope with any environmental conditions encountered during deorbit without loss of function as defined by these requirements (micrometeorites and debris flux, thermal, radiation, atmospheric drag).

BB15-OHB-05 Re-entry time. *The total time to re-entry shall be less than 25 years for a fully passive system and less than 2 years (threshold), 1 year (goal) if some active functionality of the satellite is still required.* It is important to distinguish between active and passive deorbiting devices. In the case of a passive device the deorbiting time is driven by the space mitigation requirements. In the case of an active device, the disposal phase shall not be the main driver for satellite reliability.

BB15-OHB-06 Commanding. *The device shall deploy upon ground command.*

BB15-OHB-07 Autonomy. *GOAL: The device shall deploy autonomously in case of a satellite failure that prevents a ground commanded deployment.*

BB15-OHB-08 Reliability. *The reliability of the deorbiting device shall be 0.9 or better for a fully passive device and 0.95 for a device which requires some active functionalities of the spacecraft.* This is the total reliability of the device including launch phase, stowed phase and deorbiting phase from reception of the deployment command (or autonomous command) to the re-entry in the atmosphere. Please demonstrate a reliability budget for the different phases and functions of the device lifecycle. – The requirement is traced from the SDM requirements. The distinction between passive and

active device is made to ensure that the SDM requirement is still met even accounting for the reliability of the rest of the satellite during the disposal phase.

BB15-OHB-09 Reliability. *The risk of premature deployment shall be lower than 0.01.*

BB15-OHB-10 Scalability. *The device shall be scalable for satellites between 10 kg and 100 kg (threshold), 400 kg (goal) deorbiting from 800 km (threshold) 1000 km (goal).*

BB15-OHB-11 Mass. *The EST subsystem mass shall be better than 5 % (threshold), 2 % (goal) of the total mass of a spacecraft for a deorbit from 800 km.*

BB15-OHB-12 Volume. *The stowed device shall be less or equal than 0.001 m^3/kg (threshold), 0.0005 m^3/kg in volume.* This is equivalent to the size of a conventional 1U (threshold), 0.5U (threshold) Cubesat for a 1 kg device. However, the dimensions may be differently proportioned.

BB15-OHB-13 Power. *The device shall have a power consumption of less than 0.1 W (threshold), 0.5 W (goal) per kg spacecraft mass.*

BB15-OHB-14 Demisability. *The device shall have a casualty area after re-entry of less than 1 m^2 (threshold), shall be fully demisable (goal).* To be demonstrated in DRAMA for an uncontrolled re-entry at Sun-synchronous inclination (break-up at 78 km).

BB15-OHB-15 Cost. *The cost of the entire device shall be lower than 100 kEUR for a 100kg satellite in an 800km SSO.* Cost scalability w.r.t. size and orbit regime shall be analysed.

3.1.3 Harmonised requirements

The harmonised requirements are as follows.

ID	Topic	Airbus	OHB	Harmonised
R001	Mass	The device mass shall be inferior to 5 kg (TBC) (BB15-ADS001).	The EST subsystem mass shall be better than 5 % (threshold), 2 % (goal) of the total mass of a spacecraft for a deorbit from 800 km (BB15-OHB-11).	The device mass shall be lower than 5 kg. *Rationale: Selected the stronger requirement (Airbus).*
R002	Volume – Dimensions	The volume of the undeployed device shall not exceeed 10 liters (TBC) (BB15-ADS002).	The stowed device shall be less or equal than 0.001 m^3/kg (threshold), 0.0005 m^3/kg in volume (BB15-OHB-12).	The volume of the undeployed device shall not exceeed volume of a 6-U cubesat. *Rationale: The point was discussed in CDF1 and 6-U cubesat volume was selected as a reasonable yet simple requirement which is also more strict than the original ones.*

R003	Sub-system	None	The EST device shall be a separate "bolt-on" subsystem with clearly defined interfaces to the spacecraft (BB15-OHB-01).	The EST device shall be a separate "bolt-on" subsystem with clearly defined interfaces to the spacecraft.
R004	States and modes	None	The EST shall have at least two discrete states, a stowed and a deployed state, and a deployment mode which sets the device from the stowed to the deployed state (BB15-OHB-02).	The EST shall have at least two discrete states, a stowed and a deployed state, and a deployment mode which sets the device from the stowed to the deployed state.
R005	Functional	The device shall be triggering through ground TC (BB15-ADS003).	The device shall deploy upon ground command (BB15-OHB-06).	The device shall be triggered by a command from the satellite. *Rationale: In CDF2 it was decided to replace "ground TC" by "satellite".*
R006	Functional	The device deployment shall be compatible with the following S/C dynamic conditions: angular rate conditons $< 2°/s$ about any spacecraft axis (BB15-ADS004).	None	The device deployment shall be compatible with the following S/C dynamic conditions: angular rate conditons $< 2°/s$ about any spacecraft axis.
R007	Functional	The deployed device shall not require any resource (e.g. power) from the spacecraft during the disposal phase (BB15-ADS005).	The device shall have a power consumption of less than 0.1 W (threshold), 0.5 W (goal) per kg spacecraft mass (BB15-OHB-13).	The deployed device shall not require any resource (e.g. power) from the spacecraft during the disposal phase. *Rationale: Selected the stronger requirement (Airbus).*

R008	Functional	None	GOAL: The device shall deploy autonomously in case of a satellite failure that prevents a ground commanded deployment (BB15-OHB-07).	For the baseline scenario, the spacecraft is active during deployment. Autonomy shall be analysed as an option. *Rationale: The point was discussed in CDF1 and more than one party foresaw autonomous deployment as challenging to achieve, given the cost, mass and volume requirement. Hence deployment autonomy was downwgraded from a strict requirement to an option to be analysed.*
R009	Performance	The device performances shall be ensured for orbits up to 850 km altitude, with any orbit inclination (BB15-ADS006).	The device shall be scalable for satellites between 10 kg and 100 kg (threshold), 400 kg (goal) deorbiting from 800 km (threshold) 1000 km (goal) (BB15-OHB-10).	The device shall be able to deorbit 200 kg (threshold), 500 kg (goal) from 850 km circular orbit. Should also analyse performance for 200 kg satellite from 1200 km altitude. *Rationale: The point was discussed in CDF1 and consensus was reached on formulation of the harmonised requirement.*
R010	Performance	Once deployed, the device shall ensure a satellite uncontrolled re-entry in less than 25 years (BB15-ADS008).	The total time to re-entry shall be less than 25 years for a fully passive system and less than 2 years (threshold), 1 year (goal) if some active functionality of the satellite is still required (BB15-OHB-05).	Once deployed, the device shall ensure a satellite uncontrolled re-entry in less than 25 years. *Rationale: Because R007 requires passive operation after deployment, the Airbus and OHB requirements are harmonised automatically.*

R011	Reliability	The reliability of the device deployment/-operations shall be superior to 95 % (TBC) (BB15-ADS009).	The reliability of the deorbiting device shall be 0.9 or better for a fully passive device and 0.95 for a device which requires some active functionalities of the spacecraft (BB15-OHB-08).	The reliability of the device deployment/-operations shall be superior to 95 %. *Rationale: Considering that R007 requires passive operation after deployment, the Airbus requirement is strictly stronger than the OHB one. Hence the Airbus requirement is taken as the harmonised one, with TBC dropped.*
R012	Safety	There shall be no spurious triggering during nominal in-orbit operations (BB15-ADS010).	The risk of premature deployment shall be lower than 0.01 (BB15-OHB-09).	The risk of premature deployment shall be lower than 0.001. No single-point failure mechanism for such event shall exist. *Rationale: It was pointed out in CDF1 that while spurious triggering is strongly to be avoided, requiring exactly zero probability for it is not feasible. The probability 0.001 was decided as a compromise.*
R013	Lifetime on ground	The device design shall be compatible of 10 years (TBC) ground storage, without need for complimentary re-acceptance testing at the end of the storage period (BB15-ADS011).	None	The device design shall be compatible of 10 years ground storage, without need for complimentary re-acceptance testing at the end of the storage period.

R014	Lifetime in orbit	The device perfomance and reliability figures shall be guaranteed during the following mission operation lifetime: 10 years for LEO missions (BB15-ADS012).	In stowed state the device shall be mounted on any outside panel of a LEO satellite during launch and operations of up to 5 years (threshold), 10 years (goal) (BB15-OHB-03). In deployed state the device shall survive until re-entry in orbital altitudes between 250 km and 2000 km (BB15-OHB-04).	The device perfomance and reliability figures shall be guaranteed during the following mission operation lifetime: 10 years for LEO missions. *Rationale: Selected the stronger requirement (Airbus). OHB's subrequirement on survival in certain altitude range was dropped because it is effectively implied by R010 and R016 alias BB15-ADS014.*
R015	Environment – Radiation	The device shall ensure the expected performance under the radiation conditions observed during the operational lifetime and the disposal phase (BB15-ADS013).	None	The device shall ensure the expected performance under the radiation conditions observed during the operational lifetime and the disposal phase.
R016	Environment – ATOX	The deployed device shall be compatible with atomic oxygen environment in the altitude range from 200 to 850 km (BB15-ADS014).	None	The deployed device shall be compatible with atomic oxygen environment in the altitude range from 200 to 850 km.

R017	Demisability	The device shall totally demise when exposed to the thermal flux from an altitude of 78 km (BB15-ADS015).	The device shall have a casualty area after reentry of less than 1 m^2 (threshold), shall be fully demisable (goal) (BB15-OHB-14).	The device shall totally demise when exposed to the thermal flux from an altitude of 78 km, or if some tether pieces survive to the ground, their impact energy must be less than 15 J. *Rationale: The point was discussed in CDF1 and it was pointed out that theoretically, some pieces of the thin tethers might survive reentry because of their low ballistic coefficient, but they do not pose any risk to people because their descent speed and impact energy would be very low.*
R018	Cost	The device cost shall not exceeed 50 k€ (TBC) (BB15-ADS016).	The cost of the entire device shall be lower than 100 k€ for a 100 kg satellite in an 800 km SSO (BB15-OHB-15).	The recurrent cost of the entire device shall be lower than 100 k€ (threshold), 50 k€ (goal) for a 200 kg satellite in 850 km SSO. *Rationale: The point was discussed in CDF1 and the harmonised text was agreed upon.*
R019	Functional	None	None	The system shall be magnetically clean. *Rationale: This was added as a new requirement in CDF2.*

3.2 Consolidated Building Block requirements specification and statement of compliance

Table 2 summarises the compliance to the requirements. The requirement texts in Table 2 are given in concise form; the official forms were given in subsection 3.1.3 above.

Table 2: Compliance of design to requirements.

	Requirement	*Status*	*Justification*
R001	Maximum mass 5 kg	Compliant	2 kg per module 5.4
R002	Maximum volume 6-U	Compliant	2-U per module 5.4
R003	Bolt-on subsystem, clear interf.	Compliant	Mech. interface 5.3.1
R004	Has stowed & deployed state	Compliant	Design concept 5.2
R005	Triggered by satellite command	Compliant	28 V DC voltage 5.3.2
R006	Up to 2°/s rotation rate	Not compliant	Does not allow rotation after deployment
R007	Passive device after deployment	Compliant	No energy storage 5.2
R008	S/C active during deployment, autonomy analysed as option	Compliant	5.2 and 6.2.14, autonomy analysis 5.3.1
R009	200 kg (goal 500 kg) from 850 km, analyse also 200 kg from 1200 km	Compliant	Table 17
R010	Deorbiting time max 25 years	Compliant	Max 11 a with 1 module, max 5.6 a with 2 modules, Table 17
R011	Reliability at least 95 %	Partially compliant	Compliant with 2, nearly compliant with 1 module 6.2.12
R012	No single-point failure for premature deployment, max prem. depl. risk 0.1 %	Partially compliant	Compliant if satellite command (5.3.2) is reliable
R013	Grond storage max 10 years	Probably compliant	No batteries or electrolytic capacitors 5.4, 6.1.4
R014	In orbit max 10 years before triggering	Probably compliant	No batteries or electrolytic capacitors, 5.4, 6.1.4
R015	Survives relevant radiation	Compliant	No sensitive components
R016	Survives ATOX above 250 km	Compliant	Aluminium tether 6.1.1
R017	No casualty risk on ground	Compliant	Demisable 5.6
R018	Max recurrent cost 100 k€ (goal 50 k€) for 200 kg, 850 km	Compliant	Table 25
R019	Magnetically clean	Compliant	Aluminium tether 6.1.1

4 Design work logic

Initially, three concepts were analysed for first-order feasibility regarding the requirements. The concepts are 1) a cold gas thrust deployed gravity-stabilised tether, 2) spin deployed tether, and 3) spring deployed gravity-stabilised tether. Of these concepts, number 3 was agreed as the baseline concept and consequently it is analysed in the subsequent sections more thoroughly than the other concepts.

4.1 Cold gas thruster deployed gravity-stabilised tether

The first concept studied was a tether which is stabilised by Earth's gravity gradient and which is deployed (pulled out) by using cold gas thrusting. A remote unit (RU) is released from the satellite, either downward or upward. The RU contains the tether reel and a cold gas (CG) thruster which pulls the tether out. After few hundred metre deployment, the gravity gradient force starts to contribute to the pull and the thruster can be switched off at some point. More than one thruster nozzle is needed so that roughly correct thrusting direction can be maintained. A sensor (for example, infrared-based Earth limb sensor) is used for determining which direction is downward (or upward). The accuracy of the sensor need not be high. The sensor data are used for commanding the thrusters so that the proper thrusting direction is achieved.

Optionally, two systems could be deployed, one downward and the other one upward from the satellite. Using two systems provides more reliability through redundancy and doubles the achievable tether length and thrust, so that two times larger masses of 800 kg or more can be deorbited. For example, with 5+5 km tether, deorbiting from 800 km to 500 km takes 4.6 years, and from 500 km to ground takes 3 years assuming ballistic coefficient of 130 kg/m^2 (Airbus requirement BB15-ADS008).

For the autonomous deployment option, one might detumble the satellite first by the CG thrusters. For typical values of the satellite's moment of inertia and distance of the device from the satellite's centre of mass, the amount of CG propellant needed for such detumbling is not excessively high.

The main issues in this deployment scheme are the following:

1. If the electron gathering surface is located in the RU, the RU's own area is not large enough at least under some plasma conditions. To resolve this, one could add a rigid deployable to the RU to increase the surface area. However, the challenge is to deploy it without producing a mechanical impulse which could risk breaking the tether. It is also a challenge to position the deployable in such as way that it does not obscure the field of view of an Earth limb or other sensor needed to sense the downward/upward direction.

2. If the electron gathering surface is located in the main satellite, then also the power source should be located there. However, this is problematic because we cannot assume availability of the satellite's power system during the deorbiting phase.

3. The cold gas thruster: Including a CG thruster system increases the cost and makes it challenging to fulfill the recurrent cost target of 100 k€ per unit.

Figure 5 shows the cold gas thruster option for gravity-stabilised tether conceptually.

4.2 Spin deployment option

The centrifugal force can be used for deploying the tether by applying the satellite's ACS to spin up the satellite. This allows us to get rid of the cold gas thruster. The two-tether option seems to be out of question, for dynamical stability reasons, with spin deployment, which is a drawback in comparison to the vertical (i.e. gravity gradient assisted) deployment concepts. The deployment dynamics depends on two parameters which vary from satellite to satellite: the moment of inertia of the satellite and the

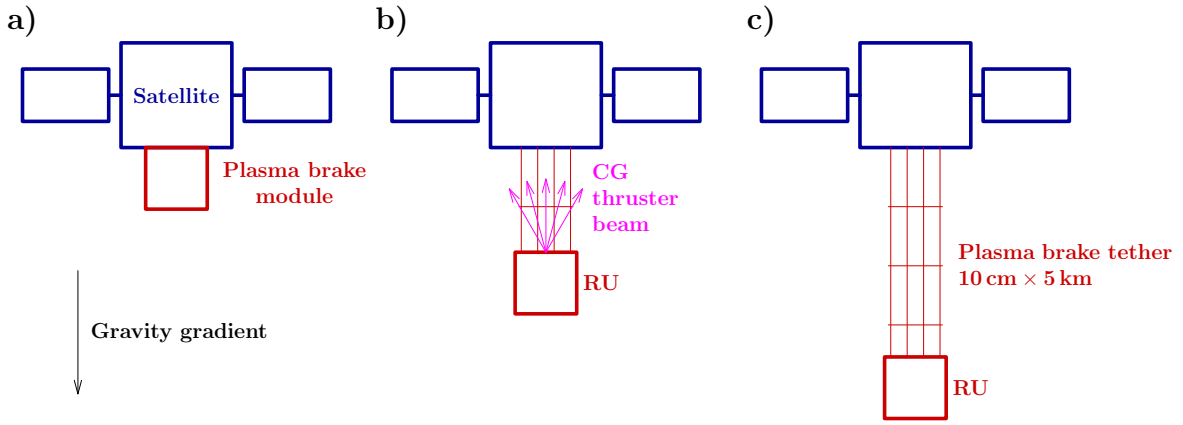

Figure 5: Cold gas thruster option for gravity-stabilised tether. a) stowed configuration, b) deployment initially by cold gas thruster residing in remote unit, c) fully deployed configuration. The thruster can be shut down after ~ 100 m when the gravity gradient tension sets in.

distance of our deorbiting unit from the centre of mass of the satellite. While not an obstacle in principle, it would necessitate an analysis of a two-dimensional parameter space and mapping the boundaries of the domain where the device is supposed to work. The electron collecting surface is also a serious issue in spin deployment, similarly to the cold-gas driven gravity-stabilised concept (subsection 4.1 above).

Figure 6 shows the spin deployment option schematically.

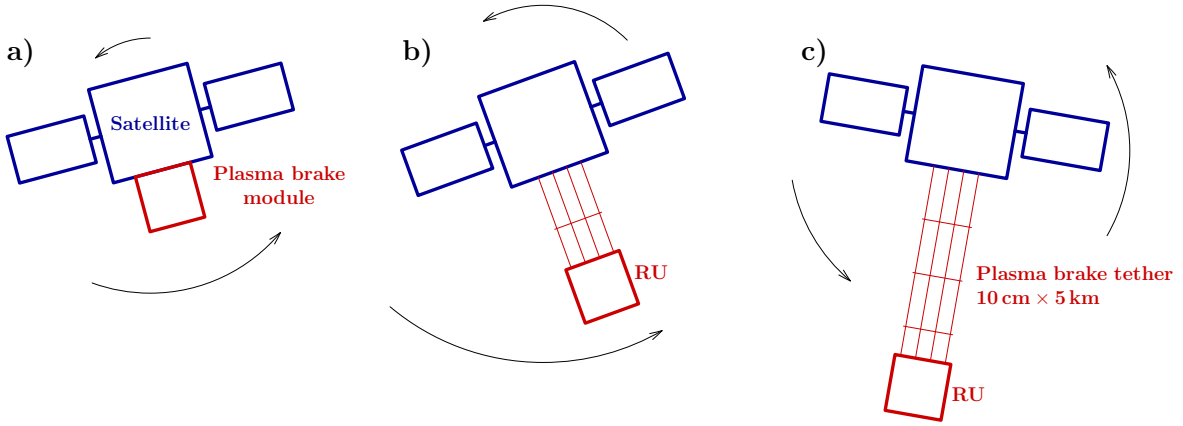

Figure 6: Spin option using the satellite's ACS. a) satellite has initiated spin as preparation to deployment, b) deployment phase during which satellite's ACS continues to add angular momentum, c) fully deployed configuration.

4.3 Spring deployed gravity-stabilised tether

This concept uses spring force instead of CG thruster to first deploy a shorter tape tether which provides separation to magnify the gravity gradient force enough to enable the deployment of the plasma brake tether. This resolves the cost issue inherent with using the CG thruster system. It turns out that also the electron collecting surface issue is naturally resolved with this concept. Because of these benefits, this is our baseline concept and we describe it in detail below, section 5.

5 Design description

5.1 Functional analysis and main problem areas identification

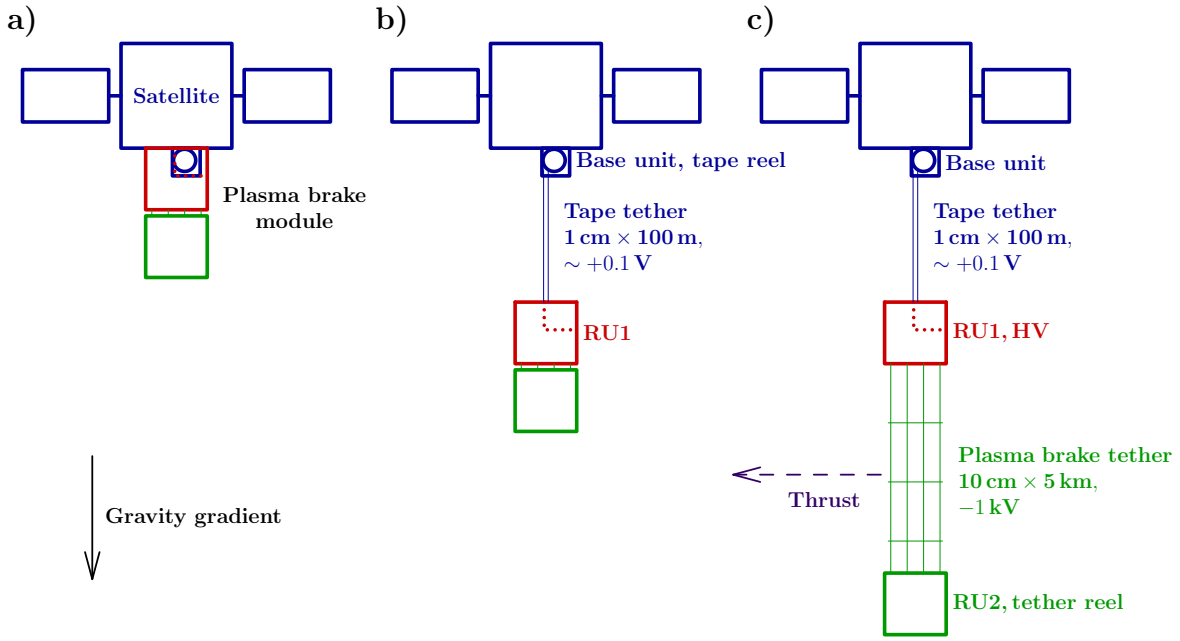

Figure 7: Schematic of the device in deployed state when deployment occurs downwards. a) stowed state, b) tape tether deployed, c) also propulsive tether deployed. The tape tether also acts as electron collecting surface.

The hardware is composed of a base unit (BU) which is permanently attached to the satellite and RU1+RU2 combination which is jettisoned by springs (Fig. 7). A 100 m long tape tether is reeled out from the BU following the jettison and gently braked so that no bounceback occurs. Later, RU1 and RU2 are separated and the maintether is deployed from RU2 between the units. A high voltage (HV) source onboard RU1 is used to keep the tether negatively charged while the tape tether provides the current balancing electron gathering surface. Also RU2 contains similar HV subsystem, which guarantees that RU2 deorbits itself quickly in case of maintether breakage.

The sequence of operations is as follows:

1. A robust plastic line which binds BU and RU2 together through a pipe passing through RU1 is melted by a resistor in RU1. Electric power from melting comes from BU through ejection springs which double as electric lines. RU1 also starts a 30 minute timer.

2. Ejection springs eject RU1+RU2 combination away and force the tape tether reel to rotate.

3. Tape tether reel continues to rotate and RU1+RU2 combination continues its flight.

4. A cycle counter onboard BU counts the cycle of the tape tether reel. When 90 % of tape tether is deployed, BU activates a gentle brake which stops the tape tether

reel nominally at 95 % deployment. This is the last operation performed by the BU.

5. When RU1's 30 minute timer expires, it melts a thinner plastic line binding RU1 and RU2 together. Electric power for the melting comes from RU1's solar panels. RU1 also switches off an internal electric path which short-circuits RU2 through brush contacts between the units and turns on its HV subsystem.

6. RU2 is now operative because voltage produced by its solar panels is no longer short-circuited through RU1. RU2 starts the reel motor and starts to deploy the maintether. The motor works whenever the unit is in sunlight.

7. A cycle counter onboard RU2 follows the progress of maintether deployment. When deployment is complete according to the counter, RU2 stops its motor and turns on the HV subsystem.

The cycle counter of BU runs only for a few minutes and is powered by the satellite.

The following logic avoids a necessity to keep the 30 minute timer chip powered during eclipse. The timer of RU1 needs to tick only in sunlight and it may reset itself in eclipse. If the deployment sequence starts in eclipse, the timer actually starts only when the satellite enters sunlight, and because the sunlit period lasts for longer than 30 minutes, the timer expires before the satellite enters eclipse again. If the deployment sequence starts soon after entering sunlight, the same happens: the expiration of the timer still occurs in sunlight. Otherwise the timer is not complete when we enter eclipse, in which case the timer restarts when the eclipse ends which yields the timer to expire in sunlight. This logic works if the timer duration is less than the shortest expected sunlit portion of the target orbit.

The cycle counter of RU2 needs to store its state in F-RAM so that the state is preserved over eclipse.

The main problem areas (which are however fully addressed by the design) were the following:

1. The required long durability which, when combined with the ambitiously low recurrent cost target, implies that any kind of onboard electric energy storage devices were to be avoided.

2. The lack of energy storage device also implies that the shape of RU1 and RU2 should be close to cubical so that solar panel power does not vary too much when the unit tumbles and turns. Likewise, all six sides of RU1 and RU2 must be covered by solar panels and the releasable docking mechanisms must comply with this.

3. The existence of potentially wide temperature changes in the stowed configuration limits the selection of components.

4. No secondary debris generation: if the maintether breaks, RU2 should deorbit itself automatically.

5. The device is passive in the sense that the satellite can passivate itself electrically 48 hours after deployment initiation. During the first 48 hours of the deployment process, the satellite's ACS must be kept on for dynamical stability reasons.

6. We make no assumptions concerning the electrical grounding plan of the host satellite. To accomplish this we use the metal-coated tape tether as the electron gathering area. Metal coating of the tape is necessary anyway to protect the tape's polyimide against ATOX.

5.2 Design concept architecture

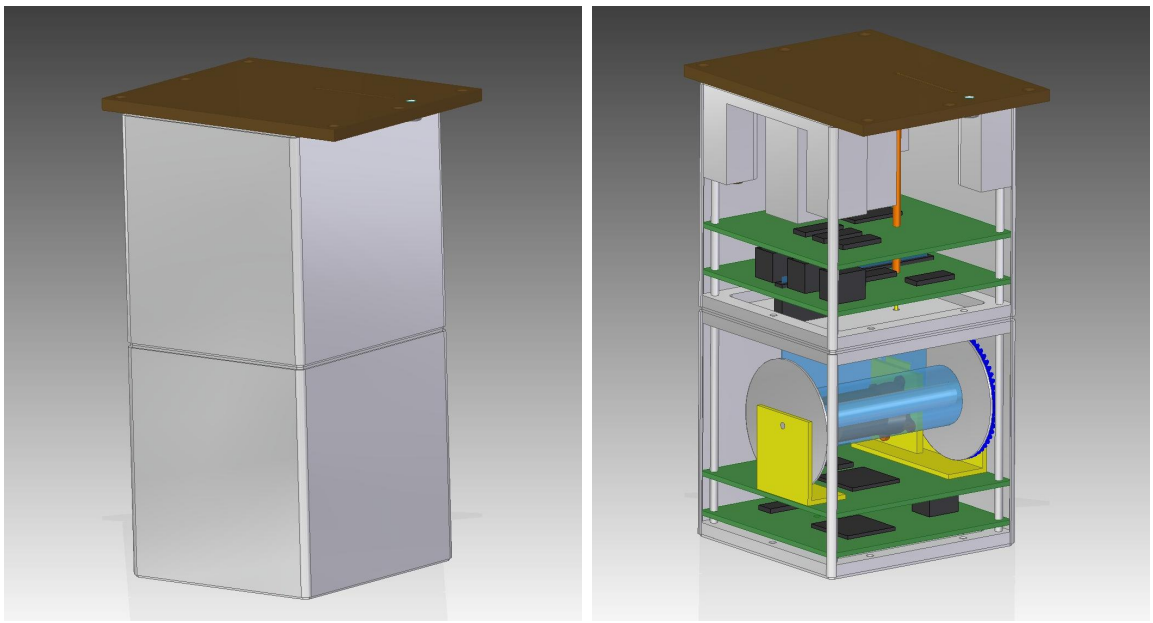

Figure 8: CAD drawing of the plasma brake module in stowed configuration with side panels installed (left) and partially opened (right).

A CAD drawing of the module is shown in Figs. 8 and 9. Figure 8 shows the stowed configuration from two sides, the units from top to bottom are the base unit (BU), remote unit 1 (RU1) and remote unit 2 (RU2). The opened view is shown in Fig. 9.

The BU (brown) is a plate which is attached to the satellite by screws. The BU also contains a downward protrusion (red; visible in Fig. 9) which contains the reel which deploys the tape tether (green; visible in Fig. 9). In stowed configuration the protrusion is inside a corresponding opening in RU1. In stowed configuration the stack BU+RU1+RU2 is held together by a plastic line which is stretched between RU2 and the BU and which passes through RU1 inside a tube (orange). In the horizontal direction, the BU and RU1 are kept together by four pins of the BU that go into corresponding holes in RU1. The pins are associated with ejection springs which cause separation of RU1+RU2 from the BU after the plastic line is melted by a resistor onboard RU1.

Both RU1 and RU2 are surrounded by solar panels on all six sides (not shown in the figures for clarity). RU1 contains to printed circuit boards, one for the electric power system and the other one for the high-voltage (HV) subsystem.

RU2 also contains similar electric power system card and HV card, plus the main tether reel and the electric motor that rotates it. The electric motor controller is included on the electric power system card. The maintether is indicated schematically in the figures by a wide sheet.

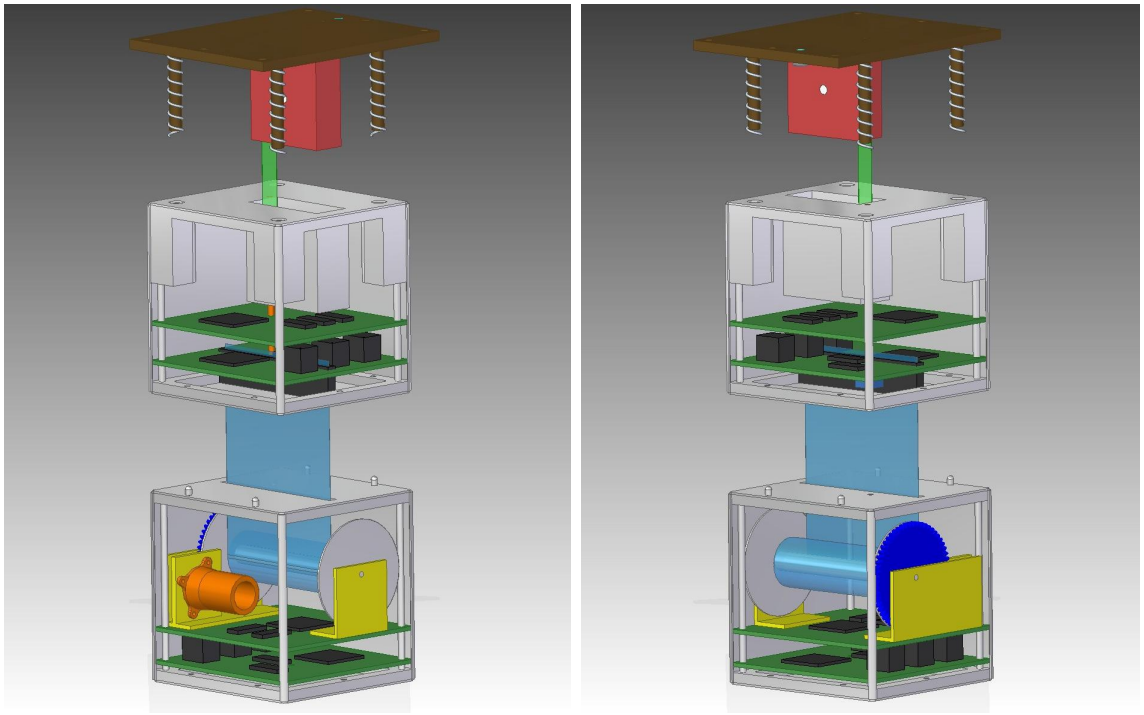

Figure 9: Plasma brake module in opened form viewed from two directions.

RU1 and RU2 are separated by melting a short plastic line which connects them. Horizontal movement between RU1 and RU2 is prevented in the stowed configuration by shallow protrusions of RU2 that go into corresponding holes in the bottom of RU1. To ensure detachment of RU1 and RU2 from each other, they are initially separated by small leaf springs installed along the perimeter of the top plate of RU2. When the first plastic line which keeps the stack together is melted, said springs force detachment by a couple of millimetres of RU1 and RU2 from each other while the second plastic line which is melted later prevents their further separation. By this arrangement, separation of the units is guaranteed without loading the maintether with any additional force.

Similarly to the first concept (subsection 4.1), we can optionally have two modules, one deployed downward and the other one upward, to increase redundancy and to double the available deorbiting thrust. The second module doubles the nominal performance and increases reliability dramatically due to redundancy.

5.3 Design concept interfaces

5.3.1 Mechanical interface

The device is bolted on the bottom or/and roof of the satellite, in principle in any free location. If there is a choice, we recommend installation on a location which is aligned with the centre of mass of the satellite (that is: draw a vertical line through the centre of mass in the satellite's nominal 3-axis stablised orientation and install the unit where the line crosses the satellite's bottom or roof panel). The centre of mass aligned installation is not needed (although it can be done if such possibility exists) in case the satellite has two modules, one deploying upward and the other one downward (which is recommended if the satellite is heavier than 300 kg or if the customer wants extra

redundancy), but then we recommend that the two units are installed along a common vertical, regardless if that vertical goes through the centre of mass or not.

The rationale is that spring deployment causes a rotational recoil of the satellite which is however zero if centre of mass aligned installation is used. The recoil is not a problem if the satellite's ACS is still working so that it can absorb the recoil. In case the ACS does not work, either centre of mass installation (in case of a single unit system) or mutually aligned shooting direction installation (in case of two-unit system) minimises the recoil effect. If the ACS does not work and the installation does not follow these guidelines, then there is a risk that the tape tether can eventually wrap around the satellite which might make deploying the propulsive tether(s) unsuccessful.

If there is only one module, if none of the above options is practical for the satellite and if one still wants to maximise chance of success in case of ACS failure, one can perform the spring ejection somewhat off-vertical direction if that makes the shooting direction align with the satellite's centre of mass. Then one needs a bracket which is installed in an oblique direction, but one gets the freedom to install the device in almost any position on the bottom or top panel without a need to go to a two-unit configuration. The shooting direction can differ from the vertical by a significant angle: the gravity gradient force acting on the RU1+RU2 combination will then slowly reorient the satellite so that the tape tether points downwards. If this strategy is used, we recommend to consider increasing the waiting time constant that elapses before detaching RU2 and starting deployment of the propulsive tether. During the waiting time, any oscillations of the tape tether should be damped.

In general, the system cannot perform reliably in a case where the satellite's ACS has died and the satellite has already started to tumble. Therefore we recommend to activate the unit quickly in case major ACS failure, of course unless the mission for some reason requires to continue operations even if ACS functions have been lost.

If a placement strategy is used which relies, in case of ACS failure, on knowing the centre of mass of the satellite, we remark that the centre of mass can often only be known accurately if the main propellant tanks are empty, that is, if the propulsion system (if any) has already been successfully passivated. Therefore, if the placement strategy relies on knowing the centre of mass (always the case in single-unit configurations), then, should the ACS fail, one should consider passivating the propulsion system before deploying the unit(s) to maximise likelihood of success.

Below (or in case of upward deployment, above) the satellite, a cone of clearance with half-angle 45° is needed to avoid the tape tether from touching any part of the satellite. In case of single-module system, the axis of the cone is the line which goes through the tape tether attachment point and the centre of mass of the satellite. In case of two-module system the cone axis is the line which connects the attachment points of the lower and upper tape tethers.

5.3.2 Electrical interface

The electric interface is a single 28 V DC voltage which, when put on, burns a deployment lock (a spring held in position by a plastic line which is cut by melting by a resistor) and thereafter provides power for the cycle counter and brake of the tape tether reel when the module is deployed, which takes a few minutes. After this the satellite can perform electric passivation.

5.3.3 Thermal interface

No thermal requirements are put to the host satellite. The plasma brake module is engineered so that it survives a wide temperature range of −55° to +100°C when attached to the surface of the satellite. When the motor and the HV sources operate, the devices will be far from the host satellite and therefore they will have normal cubesat-like internal temperature of ∼ 10°C.

5.4 Design concept performance and budgets

The mass budget of the base unit (BU) and the two remote unit (RU1, RU2) are shown in Tables 3–5. The mass budgets are based on typical CubeSat material choices and material thicknesses, and particular mass optimisations were not made. The margin philosophy is 5 % for off-the-shelf items, 10 % for off-the-shelf parts requiring minor modification and 20 % for new designs [AD2].

Table 3: Base unit mass budget.

Part	Material	Mass [g]	Margin	Mass /w margin [g]
Frame	Al	179.0	10 %	196.9
6 M6x15 mounting screws	SS	33.6	5 %	35.3
Tape reel	Plastic	4.4	20 %	5.3
Tape reel axis	Al	0.9	20 %	1.1
Tape reel enclosure	Plastic	8.8	20 %	10.6
Brake mechanism		3.0	20 %	3.6
Cycle counter		2.0	20 %	2.4
Tape	Kapton	19.0	20 %	22.8
Cables and harnesses		10.0	20 %	12.0
Springs	SS	4.5	10 %	5.0
Screw M4x4	SS	1.7	5 %	1.8
		266.9		296.8

Table 4: RU1 mass budget.

Part	Material	Mass [g]	Margin	Mass /w margin [g]
Frame	Al	87.2	10 %	95.9
1.0 mm side panels	Al	96.1	5 %	100.9
6 side solar panels		174.0	5 %	182.7
Top and bottom panels	Al	67.1	10 %	73.8
EPS PCB		47.0	20 %	56.4
HV PCB		55.0	20 %	66.0
8 M3x8 screws	SS	8.6	5 %	9.0
Cables and harnesses		8.0	20 %	9.6
Other structural		14.0	20 %	16.8
		557.0		611.1

The total mass with margins is 1907.93 g which is well below the 2.5 kg goal for a single module. A ballast mass of 149.82 g is included in RU2 to raise the total mass of

Table 5: RU2 mass budget.

Part	Material	Mass [g]	Margin	Mass /w margin [g]
Frame	Al	87.2	10 %	95.9
1.0 mm side panels	Al	96.1	5 %	100.9
6 side solar panels		174.0	5 %	182.7
Top and bottom panels	Al	67.1	10 %	73.8
EPS PCB		47.0	20 %	56.4
HV PCB		55.0	20 %	66.0
Motor phySPACE19		55.0	5 %	57.8
Motor driver electonics		30.0	20 %	36.0
Tether reel	Al	30.7	20 %	36.8
Tether reel mount	Plastic	17.0	20 %	20.4
Pinions	Plastic	9.0	20 %	10.8
Tether 5 km, 5×35 μm	Al	65.0	20 %	78.0
8 M3x8 screws	SS	8.6	5 %	9.0
Cables and harnesses		8.0	20 %	9.6
Other structural		14.0	20 %	16.8
Ballast mass		–	–	149.1
		763.7		1000.0

RU2 to 1.0 kg. This mass is used to provide sufficient gravity gradient tension for the tether.

The plastic parts are mostly TecaPEEK plastic.

The mass of RU1 should be minimised because the smaller it is, the smaller are tether oscillations because the inertia of RU1 tends to amplify them. In dynamical simulations (6.2.13) we use 0.5 kg for RU1 mass. Our current estimate of 0.611 kg (including margins) exceeds this by 111 grams. If mass optimisation is performed, one should concentrate on RU1. One can also optimise the mass of BU if one wants, but it only affects the launch mass, not the dynamical properties.

The design uses standard CubeSat frame dimensions so that the side panels, solar panels and PCBs can be standard off-the-shelf CubeSat parts.

The ballast mass of RU2 is put at the bottom because dynamical simulations show that stability is improved if the centre of mass of RU2 is positioned as far away as feasible from the maintether attachment point (6.2.13). One could also try to use the ballast mass for mechanical damping to damp tether oscillations, but this possibility is not explored further here because according to dynamical simulations, the most efficient way to improve stability is to curl up the load-bearing tether wire to decrease the effective Young modulus of the tether (see 6.2.13).

5.5 System level impacts

Our requirements for the satellite system are the following:

1. If we decide to use nickel as the tether material, it is a ferromagnetic substance and thus in that case the satellite is not magnetically clean. Other reasonable tether material candidates are not ferromagnetic.

2. The satellite's ACS must actively absorb angular momentum produced by spring ejection. The amount of angular momentum depends on placement of module with respect to centre of mass of satellite. For fuller discussion about this issue, see subsection 5.3.

5.6 Inputs for demisability analyses at system level

The unit is made of two cubesat-type boxes which surely burn completely in the atmosphere because they do not contain any titanium tanks or other similar components which might survive reentry.

Some parts of the opened tether might in theory survive reentry because the tether wires have a low ballistic coefficient of order 0.1-0.4 $\mathrm{kg/m^2}$. The speed of descent of the $\sim 25\,\mu$m wide metal wires the lower atmosphere is of order 1 m/s. Such potentially falling thin wires are safe because the impact energy per metre is of the order of some microjoules[1].

If the device does not operate properly and consequently the tether does not open from the reel and if the tether is made of high melting point material, then the spool containing the reel might in theory survive reentry. The maximal mass of such unopened tether reel is about 0.2 kg and its surface area at least about 10 $\mathrm{cm^2}$ (in the worst case, i.e. if it falls the narrow end downward). This yields a ground descent speed of about 40 m/s and maximal impact energy of 160 J which exceeds the 15 J safety limit tenfold.

6 Design justification

6.1 Solutions trade-off

6.1.1 Material selection

Analysis of candidate materials is presented later in subsubsection 6.2. Here we motivate the selection of the tether material which arises from that analysis.

Aluminium (more specifically: alloy which has 99 % of aluminium and 1 % of silicon) was the first material with which Coulomb drag tethers were produced. Unfortunately, this production process, although workable and at TRL 4, is inherently somewhat costly, because it needs specific aluminium bonding wire and fine mechanical parts which need regular servicing (e.g., cleaning of the bonding wedge). However, other production processes (currently at TRL 1) could probably also be applied for aluminium. Overall, aluminium is our baseline tether material.

Gold would be a conservative material choice. It is mechanically weak, but tolerates ATOX very well (gold is the only metal that basically does not form any oxides at all) and has TRL 3 in tether manufacture. Gold is also expensive, but the amount needed is small. The current cost of gold contributes 8700 € to the cost of a 5 km long tether.

For other metals and alloys, the TRL of production is low at the moment. Assuming that production can be accomplished, nickel would be a reasonably good choice, but it has the drawback of being ferromagnetic so that if one uses nickel tethers, the satellite would be hard to make magnetically clean, if magnetic cleanliness is a requirement for

[1] Should someone find such reentered tether piece, it could become a valuable collector's item!

the mission. Copper would be otherwise a good material, but it may have a problem with ATOX. Most or nearly all strongly alloyed metals such as Inconel and stainless steel have the problem of having low electrical conductivity. Regardless of alloying, titanium also has rather poor electric conductivity.

The different parameters are interrelated in the sense that if mechanical strength and conductivity are high, one can make the tether longer (without risking it to break due to the gravity gradient force and without risking the ohmic loss becoming too high fraction of the voltage) whence it brings the satellite of given mass down faster. A shorter deorbiting phase decreases the problem of sputtering proportionally. Because of these considerations, under the assumption that TRL of production technology could be increased, we recommend aluminium and nickel as the secondary material choice.

Table 6 summarises benefits and drawbacks of some tether materials. Double minus evaluation in any property excludes the material from total score ranking (bottom section). We evaluate mechanical strength at the (maximum) equilibrium temperature: it defines how long the tether can be. Electrical conductivity is also important and if it is too low, it also limits the attainable maximum length of the tether. Tolerance towards erosion by ion sputtering is also a consideration and this is discussed in more detail in subsubsection 6.2.2 below. Atomic oxygen (ATOX) tolerance is also necessary and for some materials it is somewhat poorly known at the moment (the question marks in Table 6 refer to this uncertainty). The current TRL of the tether manufacturing technology is also a consideration, as is the raw material cost (it becomes relevant in case of gold). For aluminium, the tether production process is at TRL 4 [13, 14], but is inherently somewhat costly because it requires fine mechanical parts which need regular servicing. For gold and silver, the production process is at TRL 3 and tends to be less costly. Silver is out of question for LEO because of its low ATOX tolerance. For other metals, the production process has not yet been studied and is at TRL 1. If a generic process would be developed, it could probably also be applied to aluminium, which could render the material again viable. Beryllium has very good mechanical, electric and sputter tolerance properties, but is inherently expensive to use because it is poisonous and carcinogenic. Beryllium also absorbs a significant fraction of incident sunlight which makes its equilibrium temperature in sunlight high, and high temperature somewhat downgrades the mechanical and electrical properties. The same is true also for copper and gold because they are coloured metals.

6.1.2 Device geometry selection

Our baseline device geometry is the spring deployment method (subsection 4.3). In this method the metal-coated tape tether provides abundant electron gathering surface without having to put any requirements to the satellite. For other geometrical options, the main problem areas are where to put the electron gathering surface so that it does not disturb other parts of the device and how to avoid the use of relatively costly CG thrusters. For the electron gathering surface, we could in principle use the satellite itself, but that would require us to put some nontrivial requirements to the satellite regarding its surface materials, grounding plan, etc. For further reasoning, see 4.1.

Table 6: Tether material evaluation. Al1Si is an alloy with 99 % aluminium and 1 % silicon used by wire bonding industry, while Al refers to generic high-strength aluminium alloy.

	Mech. strength	Elec. cond.	Sputter tol.	ATOX tol.	Magn. clean	Mat. cost	TRL	Tether cost	**Tot. score**
Al1Si	0	+	+	+	+	0	4	-	3
Au	-	0	-	++	+	-	3	0	0
Al	0	+	+	+	+	0	1	0	4
Ni	+	0	0	+	0	0	1	0	2
Cu	+	+	-	- -	+	0	1	0	- -
Rh	?	0	-	+	+	- -	1	0	- -
SS	+	- -	0	+	+	0	1	0	- -
Inconel	+	- -	0	+	+	0	1	0	- -
V	?	- -	+	+	+	0	1	0	- -
Ti	++	- -	+	+	+	0	1	0	- -
Ta	?	- -	0	+	+	0	1	0	- -
Zr	?	- -	+	+	+	0	1	0	- -
Hf	?	- -	0	+	+	-	1	0	- -
Mn	?	- -	-	+	+	0	1	0	- -
Cr	- -	-	0	+	+	0	1	0	- -
Ir	?	- -	-	+	+	-	1	0	- -
Pd	?	- -	-	+	+	-	1	0	- -
Pt	?	- -	-	+	+	-	1	0	- -
W	?	-	0	+	+	0	1	0	- -
Mo	- -	0	0	+	+	0	1	0	- -
Co	?	-	0	+	0	0	1	0	- -
Ru	?	-	-	+	+	-	1	0	- -
Ag	0	+	-	- -	+	0	3	0	- -
Be	++	+	++	0?	+	- -	1	- -	- -

6.1.3 Minimum tether tension in deployment phase

The propulsive tether needs to have some minimum tension when it is reeled out, because if it has absolutely no tension, it does not even straighten up and its shape would be unpredictable. In the aluminium tether technology[13, 14], it was found experimentally that about 0.1 cN force is enough to ensure that the tether comes out of the reel reliably. Different ways of producing the tether may yield different values. Furthermore, to enable almost zero force deployment one could use a capstan reel which pulls the tether out actively. Prototyping work and experiments would be needed to explore these options.

The minimum tether tension occurs when RU2 has separated from RU1 and deployment of the tether has just begun. At this moment the tension is created by the mass of RU2 plus the tether, acted by the gravity gradient at the tape tether length distance from the centre of mass of the system. The gravity gradient force is given by

$$F_g = mg\left(\frac{3h}{r}\right) \tag{1}$$

where m is the mass, g is the local gravity field of the Earth ($g = 7.74\,\mathrm{m/s^2}$ at 800 km altitude), h is the distance of the mass from the centre of mass of the system and r is the geocentric distance ($r = R_E +$ altitude where $R_E = 6371\,\mathrm{km}$ is the Earth radius). Besides the gravity gradient force, this formula also includes (in the factor "3") the effect of the centrifugal force which is due to the tether rotating at the orbital frequency. For example, if the tape tether length is $h = 100\,\mathrm{m}$, the mass of RU2 plus the tether mass is 1 kg and altitude is 800 km, we obtain $F_g = 0.032\,\mathrm{cN}$, i.e. one third of the 0.1 cN tension which was found reliable with the wire-to-wire ultrasonically bonded aluminium tether [13, 14]. When the 5 km tether has been fully deployed, the tension becomes 1.6 cN.

Two parameters affect the minimum tether tension: the combined mass of RU2 and the undeployed tether, and the length of the tape tether. Increasing the length of the tape tether would be a technically simple way of increasing the minimum tether tension, but it carries the drawback of somewhat increasing the cross section of the satellite in deorbiting phase and thus the risk of generating secondary debris by collision with pre-existing objects. Although the increase is still smaller than the satellite's own cross section, taking that approach is not very attractive.

Increasing the mass of RU2 would also be possible, but it cannot be increased very much or otherwise the tether tension at the end of deployment becomes inconveniently high for the tether to bear. This is a relevant point especially if the tether is made of gold because it is a mechanically weak material.

The most attractive way to proceed, in our view, is to develop tether production and deployment technology which can cope with 0.03 cN or even smaller tension. Although such technology is presently at low TRL, developing it is probably not hard and having it available would free us from making difficult tradeoff decisions between device reliability and risk of generating secondary debris. Should such development fail, one can fall back to the present solutions which involves the tradeoff.

Our baseline is to have 100 m length for the tape tether and to make the deployment apparatus such that the resulting gradient force is sufficient to deploy the tether.

6.1.4 To use a battery or not

If we use a battery in RU1 (and possibly also in RU2), we can generate thrust also during eclipse. We have flight experience of a lithium-ion battery of suitable size which flew with the ESTCube-1 cubesat, and it worked in orbit for two years (and was still working when the satellite was shut down). However, we have the requirement that the device must tolerate 10 years of ground storage followed by 10 years of orbiting until the device is turned on. Also the number of charging/loading cycles (i.e. the number of orbits) becomes large (of order 25,000) if deorbiting lasts for example 5 years. It seems challenging to guarantee that commercial lithium-ion batteries would necessarily meet such requirements.

For space use, long-life nickel-hydrogen batteries have flown successfully, for example with the Hubble Space Telescope where they worked nearly 20 years in orbit. However, to our knowledge nickel-hydrogen batteries are not available in small units and even if they were, they might be too expensive for our purpose here (less than 100 k€ total recurrent cost for the entire unit).

If one uses a battery, it might also be necessary to load and unload it every now and then during the active phase of the mission (for example once per year) to maintain

it in good condition electrically. This would be possible, but it would complicate the interface and put a small extra burden to operating the satellite.

If we do not use a battery, deorbiting lasts maybe $\sim 30\,\%$ longer. Theoretically, one might fear that turning propulsion on and off once per orbit could eventually produce some resonance tether oscillations. We do not think that this is likely, because the frequency of pendulum oscillation for the tether is $\sqrt{3}$ times higher than the orbital frequency. Because the ratio of the frequencies is an irrational number, invoking a resonant interaction is not likely. The dynamical simulations (6.2.13) confirm this hypothesis.

Because of these considerations, our baseline is to not include a battery. In case a suitable battery is found, adding it to the design is simple. The design is not mass-constrained at the moment and is unlikely to become so.

6.1.5 The mass of RU2

The RU2 hosts the motorised tether reel and a HV source which acts as partial backup for the primary HV source located in RU1 (and which also helps ensure that RU2 deorbits itself quickly in case the tether breaks). The mass of RU2 is also the ballast mass which gives the propulsive tether its tension due to the gravity gradient force. Based on the simulations (6.2.13), in this study we aim to designing RU2 so that its mass is about 1 kg, i.e. neither much larger nor much smaller. The tether reel and the HV source could probably also be fitted into a smaller mass, however, this would reduce the gravity gradient force at the start of deployment of the propulsive tether. This could be balanced by increasing the length of the tape tether, but doing so would raise the potential issue of secondary debris generation. The potential mass saving would be of order 0.5 kg per module. In this study we skip this kind of optimisations and simply aim to make a ~ 1 kg RU2, which also simplifies its design work and allows us e.g. to add some extra aluminium for radiation protection and for mechanical robustness.

RU1 does not have a ballast role and therefore normal mass optimisation philosophy applies to it (i.e. the usual tradeoff between reliability, production cost and mass minimisation).

Our baseline is to have RU mass of 1.0 kg.

6.2 Analyses, simulations and test results

6.2.1 Conductivity

Table 7 lists conductivities of unalloyed metals and also conductivity divided by density. Unalloyed metals are typically soft and to increase their tensile strength it is necessary to use some alloying, while alloying generally decreases the conductivity. We can use Table 7, however, to exclude or at least cast doubt on those materials that have low conductivity per density even in unalloyed state.

6.2.2 Sputtering

Table 8 lists sputter yields for metals when bombarded by 1 keV oxygen, hydrogen and helium atoms or ions. Sputtering by hydrogen and helium is generally insignificant

Table 7: Conductivity and conductivity divided by density. Second column is sputtered mass per incident 1 keV O+ from Table 9.

	$m_{\text{sp.}}$ [u]	σ [$10^7\Omega^{-1}\text{m}^{-1}$]	σ/ρ [$10^3\text{m}^2\Omega^{-1}\text{kg}^{-1}$]
Beryllium	8.0	2.8	15
Aluminium	27	3.5	13
Copper	94	6.0	6.7
Gold	213	4.1	2.1
Rhodium	80	2.3	1.9
Molybdenum	39	1.9	1.8
Cobalt	49	1.6	1.8
Nickel	52	1.4	1.6
Chromium	57	0.8	1.1
Ruthenium	76	1.4	1.1
Tungsten	61	1.9	1.0
Iridium	117	2.1	0.93
Steel 1010	51	0.7	0.89
Vanadium	29	0.5	0.83
Palladium	121	0.95	0.80
Niobium	40	0.66	0.77
Titanium	20	0.24	0.53
Tantalum	50	0.76	0.46
Platinum	126	0.9	0.42
Zirconium	35	0.24	0.37
Rhenium	84	0.52	0.25
Hafnium	67	0.30	0.23
Manganese	85	0.07	0.1

and oxygen is considered in the following. The sputter yield is the averaged number of atoms eroded from the surface per impact.

Table 8: Sputter yields of some metals at 1 keV [16].

		O atom	H atom	He atom
Al	Aluminium	1.002	0.022	0.189
Be	Beryllium	0.892	0.022	0.187
Cu	Copper	1.477	0.026	0.254
Au	Gold	1.08	0.005	0.151
Rh	Rhodium	0.777	0.004	0.100
Mo	Molybdenum	0.408	0.002	0.049
Co	Cobalt	0.839	0.012	0.135
Ni	Nickel	0.894	0.013	0.145
Cr	Chromium	1.099	0.017	0.183
Ru	Ruthenium	0.750	0.003	0.089
W	Tungsten	0.334	0.0	0.025

Because densities and atomic masses differ widely, the sputter yield does not directly tell how much the surface is eroded. A better measure than the raw yield is the volume, or even better, the mass of material eroded per impact. The volume can be computed by multiplying the sputter yield by the atomic mass and dividing by the material density. This information is given in Table 9.

Table 9: Sputter-eroded volume (in cubic ångström) and mass (in atomic mass unit u) of material per incident 1 keV O+ ion.

	Sp. yield	m_{atom}[u]	ρ[kg/m^3]	Sp.vol.[10^{-30} m^3]	$m_{\text{sp.}}$[u]
Beryllium	0.892	9.0	1850	7.2	8.0
Aluminium	1.002	27.0	2700	16.7	27
Copper	1.477	63.5	8960	17.5	94
Gold	1.08	197	19300	18.4	213
Rhodium	0.777	102.9	12400	10.8	80
Molybdenum	0.408	96	10300	6.4	39
Cobalt	0.839	58.9	8900	9.3	49
Nickel	0.894	58.7	8900	9.8	52
Chromium	1.099	52	7200	13.3	57
Ruthenium	0.750	101	12450	10.2	76
Tungsten	0.334	184	19250	5.3	61

Table 9 is sorted by the sputter mass (last column). If one keeps the wire thickness fixed, the sputter volume tells the material ranking concerning sputtering. Instead, if one lets wire thickness vary and instead keeps the mass per unit length constant (because the wire mass per unit length is what measures the potency of damage to other space assets), then one should instead rank by materials by the sputtered mass, as is done in Table 9. In this ranking, beryllium (8) would be by far the best material, primarily because beryllium atoms are very lightweight, and gold (213) would be by

far the worst. Aluminium is good (27), nickel moderate (52) and copper relatively bad (94).

One has to note, however, that if a material has high tensile strength and high conductivity, it would enable us to make the tether longer. With longer tether, the deorbiting process is shortened and sputtering erosion is correspondingly reduced.

For gold, for example, the sputter yield of 1.08 per oxygen atom is equivalent to 0.61 μm erosion rate per year in pure oxygen plasma with $3 \cdot 10^{10}$ m^{-3} density and -1 kV tether voltage. Over a five-year deorbiting phase, for example, this erosion rate corresponds to 3 microns per year so that a 25 μm diameter wire becomes a 19 μm wire, thus losing 43 % of its material.

Deorbiting from a higher altitude such as 1200 km where the plasma is mostly hydrogen is not more susceptible to sputtering than from a lower altitude, even if deorbiting takes longer than 5 years.

Deorbiting can also be prolonged due to lower solar activity as the plasma density is then lower and its oxygen abundance is less. Again, however, the prolonged duration does not translate to increased sputter erosion because the plasma is more hydrogen-rich. Thus to get an idea of the effect of sputtering, to first approximation it is sufficient to assume some average properties of the ionosphere. If the true plasma conditions differ, deorbiting may happens faster or slower, but the effect of sputtering stays roughly the same.

6.2.3 ATOX tolerance

Aluminium and most other metals tolerate ATOX well, with the exceptions of silver whose tolerance is bad and copper which is also probably susceptible to damage at least when the ATOX dose is high [2]

6.2.4 Mechanical strength

We require high tensile strength in a rather wide temperature range, roughly $-100..+100^\circ$ C, and possibly higher for coloured metals because they absorb more sunlight. Typically all metals emit poorly in the infrared so their equilibrium temperature are high in sunlight. Coatings are not effective for increasing the infrared emissivity in our case, because the wires are slowly eroded by ion sputtering and thus any coating is likely to be lost during the service life[3] Beryllium is an example of a metal which becomes especially hot in sunlight because it emits poorly in infrared while absorbing $\sim$ 50 % of the solar radiation. The tensile strength and electrical conductivity of metals tend to decrease when temperature is increased, so if a metal has naturally high equilibrium temperature in sunlight, this should be taken into account when comparing its mechanical and electrical properties of competing materials.

Overall the issue of mechanical strength is a complicated one because the mechanical properties of a metal depend not only on the alloying ingredients, but also on the heat treatment and cold working applied. Furthermore, the technique used for wire-to-wire bonding in making the tether affects the strength, because a chain is as strong as its weakest link.

[2]Telecon held with Adrian Tighe, Thomas Rohr and Julian Austin on November 2, 2016.

[3]However, a coating could be useful against potential cold welding on the reel before deployment.

6.2.5 Low-temperature ductility

Some metals such as molybdenum and tungsten and some steel alloys become brittle at low temperature. Copper, nickel, aluminium, gold, silver and titanium based metals as well as some stainless steels are examples of materials where a brittle-ductile transition generally does not occur or is safely below the lowest temperature that the wire might encounter in LEO.

It is advantageous even if not strictly necessary to use a material that has no brittle-ductile transition in any temperature. Generally, metals with face-centred cubic (FCC) crystal structure do have this property [15]. The crystal structures of metals are shown in Table 10. The FCC metals comprise aluminium, copper, nickel, silver, gold and the platinum group metals palladium, rhodium, platinum and iridium. In addition, calcium and strontium have FCC lattice, but they are not suitable because they react strongly with oxygen. Stainless steel is also ductile at low temperature, but its electrical conductivity is poor. Silver is out of question because it does not tolerate ATOX. Copper is also at least somewhat risky in terms of ATOX. Thus, if one does not want to use gold and platinum group metals because of their high cost, this leaves us only aluminium and nickel. Of these, aluminium is better in the sense that it is not ferromagnetic and has higher electrical conductivity per density. The drawback of aluminium is that its tolerance of high temperature is not very good. Nevertheless, the maximum temperature in LEO for aluminium probably does not increase much above 100°C, and this is still acceptable at least for some aluminium alloys. Nickel's temperature tolerance is much better. Its main drawback is that it is ferromagnetic and its conductivity per density is less than for aluminium, although still reasonably good. In terms of tensile strength per density, nickel and aluminium are roughly equally good. Nickel's fatigue tolerance is probably better than for aluminium.

6.2.6 Material cost

Tether material cost is typically not a driver for material selection for most of the technically viable materials. Among the more expensive materials is gold. The cost of gold ($\sim$ 30 k€/kg) is a drawback, but not a show-stopper. The same is true for ruthenium. We exclude rhodium, however, because although presently it costs about the same as gold, it has experienced about ten times higher peak prices within the last ten years. Platinum, iridium and palladium might also be too expensive, but they were already ranked down by their relatively low electrical conductivity.

6.2.7 Formula for predicting the thrust

For a negatively charged tether in streaming plasma, the Coulomb drag thrust per unit length of tether is [6]

$$\frac{dF}{dz} = 3.864 \times P_{\mathrm{dyn}} \sqrt{\frac{\epsilon_{\mathrm{o}} \tilde{V}}{e n_{\mathrm{o}}}} \exp\left(-V_i/\tilde{V}\right) \tag{2}$$

where $P_{\mathrm{dyn}} = m_i n_{\mathrm{o}} v_{\mathrm{o}}^2$ is the dynamic pressure, m_i is the ion mass ($m_i = 16$ amu for oxygen plasma here), v_{o} is the plasma flow speed relative to spacecraft (assumed to be

Table 10: Crystal structure of metals. FCC=face-centred cubic, HCP=hexagonal close-packed, BCC=body-centred cubic, TETR=tetragonal. The qualifications good, bad etc. refer to ductility at low temperature.

Aluminium	FCC	Good
Copper	FCC	Good
Silver	FCC	Good
Nickel	FCC	Good
Austenitic steel	FCC	Good
Gold	FCC	Good
Platinum	FCC	Good
Iridium	FCC	Good
Palladium	FCC	Good
Rhodium	FCC	Good
Beryllium	HCP	Probably OK
Titanium	HCP	Probably OK
Cobalt	HCP	Probably OK
Zirconium	HCP	Probably OK
Rhenium	HCP	Probably OK
Ruthenium	HCP	Probably OK
Hafnium	HCP	Probably OK
Martensitic steel	Martensite	Bad
Molybdenum	BCC	Bad
Chromium	BCC	Bad
Vanadium	BCC	Bad
Niobium	BCC	Bad
Manganese	BCC	Bad
Tantalum	BCC/TETR	Bad
Tungsten	BCC	Bad

perpendicular to the tether or else v_o denotes only the perpendicular component),

$$\tilde{V} = \frac{V_0}{\ln(\lambda_D^{\mathrm{eff}}/r_w^*)}, \tag{3}$$

r_w^* is the tether's effective electric radius [1, appendix A], $\lambda_D^{\mathrm{eff}} = \sqrt{\epsilon_\mathrm{o} V_0/(en_\mathrm{o})}$ is the effective Debye length and $V_i = (1/2)m_i v_\mathrm{o}^2/e$ is the bulk ion flow energy in voltage units. The effective electric radius is approximately given by $r_w^* = \sqrt{br_w}$ where r_w is the tether wire radius, typically 12.5-25 μm, and b is the tether width, typically 2 cm (a rough value of b is sufficient to know because r_w^* enters into Eq. (2) only logarithmically).

Equation (2) shows that the thrust is proportional to the plasma mass density $m_i n_\mathrm{o}$. Ionospheric plasma consists mainly of atomic oxygen ions, protons and also some helium ions. Hence, oxygen-rich plasma is beneficial for the plasma brake thrust because the mass of oxygen atom is 16 times larger than the proton mass.

When the dominant component of the geomagnetic field is along the tether, the thrust is reduced moderately ($\sim$ 27 %) relative to Eq. (2). For a vertical gravity-stabilised tether in polar orbit, this happens in high latitudes.

For example in O^+ plasma with typical $3 \cdot 10^{10}$ m^{-3} density and using 1 kV voltage, the thrust predicted by (2) is 85 nN/m. With this thrust, a 5 km long plasma brake tether can produce 0.43 mN breaking force, which is enough to reduce the orbital altitude of a 260 kg debris mass by 100 km per year.

6.2.8 Plasma conditions in orbit

The thrust depends on plasma density n_o and on the chemical composition through the mean ion mass m_i. Tables 11, 12, 13 and 14 show the plasma density, the fractions of oxygen, hydrogen and helium ions and the mass density $\rho = m_i n_\mathrm{o}$ (in units of proton mass m_p) as function of magnetic latitude. The averages are also shown at the last row[4]. The data are based on the International Reference Ionosphere (IRI) model version 2007 [17]. Geomagnetic longitude in Tables 11–14 was arbitrarily fixed at 40°. The summary lines nof Tables 11–14 show how the latitude-averaged plasma mass density ρ decreases when the altitude increases. If turned to effective oxygen ion density (a rough proxy for plasma brake thrust), the latitude-averaged density is $13.6 \cdot 10^{10}\,\mathrm{m}^{-3}$ at 600 km, $3.57 \cdot 10^{10}\,\mathrm{m}^{-3}$ at 800 km, $0.86 \cdot 10^{10}\,\mathrm{m}{-3}$ at 1000 km and $0.36 \cdot 10^{10}\,\mathrm{m}^{-3}$ at 1200 km.

The ionospheric plasma properties also depend on the longitude. This variation is shown in Table 15 for 1000 km altitude. Polar orbiting satellites typically sample all longitudes rather uniformly in the deorbiting phase, because orbit lowering typically erases any sun-synchronous property that the original orbit may have had. The longitude-averaged ρ at 1000 km ($4.88 \cdot 10^{11} m_p/\mathrm{m}^3$) is 2.11 times larger than the value at longitude 40° ($2.31 \cdot 10^{11} m_p/\mathrm{m}^3$) which was used as an exemplary value in Tables 11–14. Hence, Tables 11–14 give a conservative estimate of the actual plasma brake thrust.

There is also a significant solar cycle dependence of the ionospheric plasma, and the dependence is stronger at higher altitudes. In Table 16 we show the yearly dependence at 800 km altitude.

[4]In Tables 11–16, ions that are neither O+, H+ nor He+ are counted as He+ in the average (last row). The error made is small and our interest is in the mean ion mass m_i rather than in chemistry.

Table 11: Dependence of n_o and plasma composition on geomagnetic latitude at 600 km (longitude=40°, epoch 20000101:0130).

lat[°]	n_o[m^{-3}]	O+[%]	H+[%]	He+[%]	ρ/m_p[m^{-3}]
0	$2.7 \cdot 10^{11}$	93	4	0	$4.03 \cdot 10^{12}$
10	$2.0 \cdot 10^{11}$	92	5	0	$2.95 \cdot 10^{12}$
20	$2.9 \cdot 10^{11}$	90	7	1	$4.21 \cdot 10^{12}$
30	$2.2 \cdot 10^{11}$	88	8	1	$3.12 \cdot 10^{12}$
40	$1.2 \cdot 10^{11}$	89	7	2	$1.72 \cdot 10^{12}$
50	$7.2 \cdot 10^{10}$	92	5	2	$1.07 \cdot 10^{12}$
60	$5.5 \cdot 10^{10}$	95	2	1	$8.39 \cdot 10^{11}$
70	$5.2 \cdot 10^{10}$	96	2	1	$8.02 \cdot 10^{11}$
80	$5.7 \cdot 10^{10}$	96	1	1	$8.78 \cdot 10^{11}$
ave	$1.5 \cdot 10^{11}$	92	5	3	$2.18 \cdot 10^{12}$

Table 12: Dependence of n_o and plasma composition on geomagnetic latitude at 800 km (longitude=40°, epoch 20000101:0130).

lat[°]	n_o[m^{-3}]	O+[%]	H+[%]	He+[%]	ρ/m_p[m^{-3}]
0	$9.0 \cdot 10^{10}$	65	30	1	$9.67 \cdot 10^{11}$
10	$7.1 \cdot 10^{10}$	60	36	1	$7.10 \cdot 10^{11}$
20	$1.0 \cdot 10^{11}$	52	43	2	$1.68 \cdot 10^{12}$
30	$8.1 \cdot 10^{10}$	44	50	6	$6.30 \cdot 10^{11}$
40	$4.5 \cdot 10^{10}$	43	48	6	$3.42 \cdot 10^{11}$
50	$2.6 \cdot 10^{10}$	54	35	8	$2.42 \cdot 10^{11}$
60	$2.0 \cdot 10^{10}$	73	18	6	$2.42 \cdot 10^{11}$
70	$1.9 \cdot 10^{10}$	86	8	3	$2.65 \cdot 10^{11}$
80	$2.1 \cdot 10^{10}$	89	6	3	$3.03 \cdot 10^{11}$
ave	$5.3 \cdot 10^{10}$	63	30	7	$5.71 \cdot 10^{11}$

For the plasma brake, the worst-case situation is to start deorbiting in the start of the declining phase of the solar cycle because then the ionospheric plasma is probably weak in the several coming years. This has relevance mainly to the high end of debris masses because for those masses the deorbiting times can become significant. However, the next solar maximum which occurs in 11 years at latest will bring the satellite down.

6.2.9 Ion current collection

To maintain the negative charge of the tether, one must overcome the ion current that the tether gathers from the plasma. Because the tether wires are thin compared to the plasma Debye length, the so-called orbital motion limited (OML) theory provides a good approximation for the gathered current (actually an upper limit, because the geomagnetic field might reduce the current somewhat, although such reduction is typically more prominent for electrons rather than ions):

$$\frac{dI}{dz} = \chi e n_o \sqrt{\frac{2eV_0}{m_i}} d_w. \tag{4}$$

Table 13: Dependence of n_o and plasma composition on geomagnetic latitude at 1000 km (longitude=40°, epoch 20000101:0130).

lat[°]	n_o[m^{-3}]	O+[%]	H+[%]	He+[%]	ρ/m_p[m^{-3}]
0	$4.3 \cdot 10^{10}$	29	66	2	$2.31 \cdot 10^{11}$
10	$3.4 \cdot 10^{10}$	27	68	2	$1.73 \cdot 10^{11}$
20	$5.2 \cdot 10^{10}$	22	73	3	$2.27 \cdot 10^{11}$
30	$4.1 \cdot 10^{10}$	16	77	5	$1.45 \cdot 10^{11}$
40	$2.2 \cdot 10^{10}$	14	76	8	$7.30 \cdot 10^{10}$
50	$1.3 \cdot 10^{10}$	21	63	14	$5.92 \cdot 10^{10}$
60	$9.9 \cdot 10^{9}$	45	37	14	$8.05 \cdot 10^{10}$
70	$9.2 \cdot 10^{9}$	73	16	7	$1.12 \cdot 10^{11}$
80	$1.0 \cdot 10^{10}$	80	11	5	$1.31 \cdot 10^{11}$
ave	$2.6 \cdot 10^{10}$	36	54	10	$1.37 \cdot 10^{11}$

Table 14: Dependence of n_o and plasma composition on geomagnetic latitude at 1200 km (longitude=40°, epoch 20000101:0130).

lat[°]	n_o[m^{-3}]	O+[%]	H+[%]	He+[%]	ρ/m_p[m^{-3}]
0	$2.5 \cdot 10^{10}$	13	82	2.9	$7.54 \cdot 10^{10}$
10	$2.0 \cdot 10^{10}$	14	80	3.5	$6.36 \cdot 10^{10}$
20	$3.1 \cdot 10^{10}$	12	82	4.6	$9.06 \cdot 10^{10}$
30	$2.5 \cdot 10^{10}$	7.8	85	6.4	$5.89 \cdot 10^{10}$
40	$1.3 \cdot 10^{10}$	6.1	83	9.7	$2.85 \cdot 10^{10}$
50	$7.8 \cdot 10^{9}$	11	71	16	$2.43 \cdot 10^{10}$
60	$5.8 \cdot 10^{9}$	34	43	20	$3.87 \cdot 10^{10}$
70	$5.5 \cdot 10^{9}$	67	18	10	$6.22 \cdot 10^{10}$
80	$6.0 \cdot 10^{9}$	76	12	7.0	$7.54 \cdot 10^{10}$
ave	$1.5 \cdot 10^{10}$	27	62	11	$5.75 \cdot 10^{10}$

Table 15: Dependence of n_o and plasma composition on geomagnetic longitude at 1000 km (latitude=0°, epoch 20000101:0130).

lat[°]	n_o[m^{-3}]	O+[%]	H+[%]	He+[%]	ρ/m_p[m^{-3}]
0	$4.6 \cdot 10^{10}$	44	51	2	$3.51 \cdot 10^{11}$
40	$4.3 \cdot 10^{10}$	29	66	2	$2.31 \cdot 10^{11}$
80	$2.9 \cdot 10^{10}$	24	72	2	$1.35 \cdot 10^{11}$
120	$1.4 \cdot 10^{10}$	38	57	2	$9.42 \cdot 10^{10}$
160	$3.5 \cdot 10^{10}$	66	29	3	$3.84 \cdot 10^{11}$
200	$5.7 \cdot 10^{10}$	72	23	3	$6.77 \cdot 10^{11}$
240	$7.2 \cdot 10^{10}$	77	19	2	$9.06 \cdot 10^{11}$
280	$6.7 \cdot 10^{10}$	83	13	1	$9.01 \cdot 10^{11}$
320	$6.0 \cdot 10^{10}$	73	22	1	$7.16 \cdot 10^{11}$
ave	$4.7 \cdot 10^{10}$	56	39	5	$4.88 \cdot 10^{11}$

Table 16: Dependence of n_o and plasma composition on year at 800 km (latitude=0°, longitude=40°, epoch=yyyy0101:0130).

yyyy	$n_o[m^{-3}]$	O+[%]	H+[%]	He+[%]	$\rho/m_p[m^{-3}]$
1990	$1.2 \cdot 10^{11}$	86	10	0	$1.66 \cdot 10^{12}$
1991	$1.2 \cdot 10^{11}$	84	12	1	$1.63 \cdot 10^{12}$
1992	$1.1 \cdot 10^{11}$	74	21	1	$1.40 \cdot 10^{12}$
1993	$5.5 \cdot 10^{10}$	34	61	2	$3.37 \cdot 10^{11}$
1994	$3.0 \cdot 10^{10}$	16	81	1	$1.02 \cdot 10^{11}$
1995	$2.3 \cdot 10^{10}$	13	84	1	$6.81 \cdot 10^{10}$
1996	$1.7 \cdot 10^{10}$	13	84	1	$5.03 \cdot 10^{10}$
1997	$1.7 \cdot 10^{10}$	13	84	1	$5.03 \cdot 10^{10}$
1998	$3.0 \cdot 10^{10}$	18	78	1	$1.11 \cdot 10^{11}$
1999	$6.3 \cdot 10^{10}$	41	54	2	$4.52 \cdot 10^{11}$
2000	$9.0 \cdot 10^{10}$	65	30	1	$9.67 \cdot 10^{11}$
2001	$9.8 \cdot 10^{10}$	64	31	1	$1.04 \cdot 10^{12}$
2002	$1.0 \cdot 10^{11}$	67	28	1	$1.10 \cdot 10^{12}$
2003	$7.2 \cdot 10^{10}$	42	53	2	$5.28 \cdot 10^{11}$
2004	$4.1 \cdot 10^{10}$	24	72	2	$1.90 \cdot 10^{11}$
2005	$3.2 \cdot 10^{10}$	15	81	1	$1.04 \cdot 10^{11}$
2006	$2.4 \cdot 10^{10}$	13	83	1	$7.08 \cdot 10^{10}$
2007	$1.9 \cdot 10^{10}$	13	83	1	$5.61 \cdot 10^{10}$
2008	$1.5 \cdot 10^{10}$	13	83	1	$4.43 \cdot 10^{10}$
2009	$1.4 \cdot 10^{10}$	13	83	1	$4.13 \cdot 10^{10}$
2010	$1.8 \cdot 10^{10}$	13	83	1	$5.31 \cdot 10^{10}$
2011	$2.7 \cdot 10^{10}$	14	82	1	$8.37 \cdot 10^{10}$
2012	$5.3 \cdot 10^{10}$	31	64	1	$3.00 \cdot 10^{11}$
2013	$5.1 \cdot 10^{10}$	28	67	1	$2.65 \cdot 10^{11}$
2014	$6.4 \cdot 10^{10}$	40	55	2	$4.50 \cdot 10^{11}$
2015	$6.0 \cdot 10^{10}$	31	64	2	$3.41 \cdot 10^{11}$
ave	$5.2 \cdot 10^{10}$	34	62	4	$4.42 \cdot 10^{11}$

Here $\chi \geq 1$ is a numerical factor which takes into account emission of secondary electrons by the impacting ions (we estimate $\chi = 2$ to be conservative, the value is likely in range 1..2) and $d_w^{\rm tot}$ is the summed diameter of the wires that make up the tether (typically $d_w^{\rm tot} = 100\,\mu$m). The result of Eq. (4) must be multiplied by the tether length to get the current. For example in O^+ plasma with $3 \cdot 10^{10}$ m^{-3} density and 1 kV tether voltage, $dI/dz = 1.05 \cdot 10^{-7}$ A/m which for 5 km tether yields 0.53 mA current. The power consumption in this case is 0.53 W.

The ion induced (i.e., ion plus secondary electron) plasma current density at the wire surface is given by

$$j_i = \chi e n_o \sqrt{\frac{2eV_0}{m_i}} \frac{1}{\pi}. \tag{5}$$

With the above numerical values, $j_i = 340\,\mathrm{A/m^2}$. This is almost an order magnitude larger than typical solar UV induced photoelectron current $\sim 40\,\mathrm{A/m^2}$ in perpendicular illumination. In the dayside, the solar photoelectron current also in principle contributes to the power consumption, but can typically be ignored in comparison with the plasma

ion current and the secondary electron contribution.

6.2.10 Balancing electron current collection

The collected ion current must be balanced by electron current collected by the tape tether or by the RU. The voltage source forces a potential difference between the propulsive tether (negative) and the RU and/or tape tether, and nature adjusts the potentials of both with respect to the plasma until the electron and ion currents match. Such adjustment happens because when a surface goes more positive with respect to plasma, its ability to collect electrons from the plasma generally increases.

Let us consider this in more detail, first in case of the tape tether. The ion current collected by the propulsive, negative tether is

$$I_i = \chi e n_\mathrm{o} \sqrt{\frac{2eV_0}{m_i}} N_w 2 r_w R, \tag{6}$$

where V_0 is the absolute value of the tether's negative voltage with respect to the surrounding plasma, N_w is the (effective) number of the subwires that the tether is made of (generally $N_w = 4$ or 5), r_w is the tether wire radius (typically $r_w = 12.5\,\mu$m) and R is the tether length (take $R = 5\,$km). The electron current collected by the tape tether is

$$I_e = e n_\mathrm{o} \sqrt{\frac{2eV_1}{m_e}} w \frac{L}{2} \tag{7}$$

where V_1 is the tape tether's positive voltage with respect to the surrounding plasma, w is the tape's width and L its length. Requiring $I_i = I_e$ and solving for V_1 yields

$$V_1 = 16 \chi^2 V_0 \frac{m_e}{m_i} \left(\frac{N_w r_w R}{wL} \right)^2 . \tag{8}$$

For example if $V_0 = 1\,$kV, $\chi = 2$, $m_i = m_p$, $N_w = 5$, $r_w = 12.5\,\mu$m, $R = 5\,$km, $w = 1\,$cm and $L = 20\,$m, we get $V_1 = 85\,$V which is OK because it is much lower than V_0 so that not much power is wasted in unnecessarily heating the tape tether by electron bombardment. This is a worst-case estimate since we used $m_i = m_p$. If $m_i = 16 m_p$ (oxygen plasma), we get $V_1 = 5.3\,$V. Furthermore, in reality our tape would be at least 100 m long so that the situation would be even better. We remark, however, that in this estimation we ignored the effect of the geomagnetic field. Depending on its orientation, the magnetic field tends to reduce the collected electron current. We will discuss this point shortly below.

If there is no tape tether but just the RU, it also gathers some electron current. This question becomes relevant in the case that the propulsive tether has been cut and the question arises if RU2 can deorbit itself reasonably rapidly using its own HV source and the remaining piece of the tether so that formation of secondary space debris is avoided in such non-nominal situation. Let us approximate RU2 by a spherical probe with radius r_SC. The formula for spherical probe current collection is [9]

$$I_\mathrm{spherical} = \left(4\pi r_\mathrm{SC}^2 \right) e n_\mathrm{o} \sqrt{\frac{T_e}{2\pi m_e}} \left(\frac{eV_1}{T_e} \right), \tag{9}$$

where $T_e = 0.1\,$eV is the plasma electron temperature and V_1 is again the probe's positive potential with respect to plasma. However, this formula holds only when r_SC is much

smaller than the plasma electron Debye length, which is a questionable assumption in the ionospheric case at least in part of the parameter range, when $r_{\mathrm{SC}} \approx 5\,\mathrm{cm}$ as for a cubesat-sized body.

6.2.10.1 Parker-Murphy theory The Parker-Murphy electron current collection [10, 9] theory takes into account the geomagnetic field. For a spherical probe the theory first defines so-called collection radius r_{coll} which is given by

$$r_{\mathrm{coll}} = r_{\mathrm{SC}} \sqrt{1 + \sqrt{\frac{8eV_1}{m_e \omega^2 r_{\mathrm{SC}}^2}}} \tag{10}$$

where $\omega = eB/m_e$ is the electron gyrofrequency (Larmor frequency) and V_1 is the potential of the probe with respect to the plasma. Then the collected electron current is calculated by

$$I_{\mathrm{spherical}} = \left(2\pi r_{\mathrm{coll}}^2\right) e n_{\mathrm{o}} \sqrt{\frac{T_e}{2\pi m_e}}. \tag{11}$$

The validity of the theory can be seen by checking the value of the so-called dimensionless magnetic field β [9] which is defined by

$$\beta = r_{\mathrm{SC}} \omega \sqrt{\frac{2m_e}{\pi T_e}}. \tag{12}$$

We find that for a cubesat-sized body in LEO, typically $\beta \approx 3$. We also need the value of the dimensionless potential ψ_p which is defined by [9]

$$\psi_p = \frac{eV_1}{T_e}. \tag{13}$$

Now V_1 is typically 1 kV and $T_e \approx 0.1$ eV so that ψ_p is large, of order 10^4. Figure 3 of Laframboise and Sonmor [9] shows that for large values of ψ_p and for β in the range 1..3, the Parker-Murphy theory is in good agreement with the more complete and more complicated Rubinstein-Laframboise theory [12]. Hence, using the Parker-Murphy theory (10)–(11) is possible in our case. We also notice by inserting typical numerical values that it is possible to neglect the term "1" inside the outer square root in Eq. (10) so that we obtain

$$\begin{aligned} I_{\mathrm{spherical}} &= (2\pi r_{\mathrm{coll}}^2) e n_{\mathrm{o}} \sqrt{\frac{T_e}{2\pi m_e}} \\ &\approx 2\pi r_{\mathrm{SC}}^2 \sqrt{\frac{8eV_1}{m_e \omega^2 r_{\mathrm{SC}}^2}} e n_{\mathrm{o}} \sqrt{\frac{T_e}{2\pi m_e}} \\ &= 4\pi r_{\mathrm{SC}} \left(\frac{1}{\omega}\right) \sqrt{\frac{2eV_1}{m_e}} e n_{\mathrm{o}} \sqrt{\frac{T_e}{2\pi m_e}} \\ &= 4 \left(\frac{r_{\mathrm{SC}} n_{\mathrm{o}}}{B}\right) \sqrt{\pi e V_1 T_e}. \end{aligned} \tag{14}$$

Then we require $I_{\mathrm{spherical}} = I_i$ where I_i is given by (6) and solve for V_1 to obtain

$$V_1 = \left(\frac{1}{2\pi}\right) V_0 \frac{(\chi e B)^2}{m_i T_e} \left(\frac{N_w r_w R}{r_{\mathrm{SC}}}\right)^2. \tag{15}$$

Equation (15) can be used to estimate how high positive potential V_1 an electron current collecting spacecraft (radius $r_{\rm SC}$) must be raised in order to balance ion current gathered by a tether in negative potential $-V_0$, length R, wire radius r_w, number of subwires N_w, when B is the local geomagnetic field, m_i the mean plasma ion mass, T_e the electron temperature and χ the coefficient of emission of secondary electrons by accelerated ions impacting the tether. Some points of the equation are noteworthy:

1. The potential V_1 is proportional to B^2 so that current balance is easier to achieve in low latitudes rather than high latitudes. The magnetic field is two times higher over the pole than at the equator so that all else being the same, V_1 is four times higher near the pole.

2. To maintain the same voltate V_1, the spacecraft radius $r_{\rm SC}$ should be scaled linearly with the tether length R.

3. Because the ion mass m_i appears in the denominator of (15), current balance is 16 times easier to achieve in oxygen plasma than in hydrogen plasma. This is understandable because hydrogen ions are more mobile than oxygen ions and hence make the negative tether collect more current.

4. In practice, of course, we do not set the voltages independently, but the voltage source fixes only the sum $V_0 + V_1$ (in fact the difference of the potentials, but we define V_0 to be positive so that the potential of the propulsive tether is actually $-V_0$). If conditions change so that electron collection becomes harder, V_1 increases and V_0 decreases until balance is achieved. Nature finds the balance of how the voltage is divided between the electron and ion gathering body.

Inserting typical numerical values, one sees that current collection by a cubesat-sized body RU2 is anyway enough to produce at least some Coulomb drag effect on the tether, although at times the voltage V_1 becomes large in comparison to the tether voltage V_0. This means that if RU2 is equipped by its own HV source, it will deorbit itself quickly in case the tether is broken.

The magnetic field generally prohibits some electrons from reaching the collecting surface because the electron Larmor radius is not very large. For a spherical probe, the restriction is obviously independent from the direction of the field. For an elongated surface like the tape tether, the magnetic field restricts the electron current the most when it's parallel to the tether. A quantitative expression that would describe the effect fully is not easy to give because the situation lacks symmetries. However, based on typical numerical values it seems that in almost all cases the tape tether is capable of collecting the needed electron current even without biasing or with mild positive biasing. Positive biasing means that the voltage of the negative tether is correspondingly reduced, which is not very severe because the Coulomb drag depends only on the square root of the voltage. If the magnetic field is exactly parallel to the tether, more severe biasing might conceivably occur. The practical significance of this is likely to be very low, however, because such cases probably do not occur and even if they do, they last only for a short time and hence do not affect the average efficiency of the deorbiting process. The bottom line is that the tape tether is a sufficient electron collector.

6.2.11 Deorbiting time

Putting the above things together, we can simulate the orbital decay using the above data on ionospheric plasma density and mean ion mass as well as the neutral atmosphere. If we use latitude-averaged values for n_o and m_i from Tables 11–14, we obtain deorbiting time results as given in Table 17 for various initial altitudes and satellite masses. Both Coulomb drag and neutral drag are included in the calculation. For the neutral drag, ballistic coefficient of 130 kg/m^2 is assumed for the satellite (which comes from the requirements). In addition, total perpendicular area of 1 m^2 is assumed for the tape tether (e.g., 1 cm times 100 m) which gives effectively 0.5 m^2 because the orientation of the tape against the ram flow is random. The tether is assumed to be 5 km long and its effective area concerning neutral drag is 0.25 m^2. For Coulomb drag, we assume maximum tether voltage of 1 kV and maximum available power of 1.5 W. When the plasma density is high, the voltage is adjusted to be less than the maximum. This power availability issue lengthens the deorbiting time only slightly because when voltage limitation sets in, the altitude is already so low that deorbiting will happen rather fast in any case. We assume that the device operates also during eclipse time. The deorbiting time is calculated until reaching 200 km altitude. The deorbiting time is given for both one and two module configurations.

Table 17: Deorbiting time in years for one and two device confugations.

Sat. mass	Init. alt.	One device	Two devices
200 kg	850 km	2.9 a	1.5 a
400 kg	850 km	5.5 a	2.9 a
600 kg	850 km	7.9 a	4.2 a
800 kg	850 km	10.1 a	5.5 a
200 kg	1000 km	5.3 a	2.7 a
200 kg	1100 km	7.8 a	4.0 a
200 kg	1200 km	11.0 a	5.6 a

We stress that the results in Table 17 are rough and preliminary and should not be considered as a guarantee that deorbiting actually happens in the indicated time, because the ionospheric conditions used in the calculations are more exemplary than representing any rigorous averaging process over latitude, longitude, altitude, solar cycle and other parameters affecting the ionosphere. Nevertheless, the results are promising in the sense that all the times are much shorter than 25 years.

6.2.12 Failure probability of deorbiting

Table 18 shows the meteoroid and debris flux for various diameter particles at 800 km altitude, which corresponds roughly the worst case. The calculation is made for MASTER-2009 version 7.02 "business as usual" debris scenario for the calendar year 2025. We use a 1 cm wide 100 m long tape tether and a 5 km long 8 cm wide wire tether made of 5 25 μm metal wires at 20 cm bonding interval. For the tape tether, the 3 mm flux is relevant. For the multi-wire tether, the 10 μm flux is relevant because it cuts the individual wires, and also the 3 cm flux plays a role because those impactors can cut the tether at one blow.

Table 18: Meteoroid and debris flux at 800 km according to MASTER-2009 model version 7.02 for year 2025.

Diameter	Flux[m^{-2} a^{-1}]	Remarks
3 cm	$1.6 \cdot 10^{-5}$	Almost only manmade
3 mm	$5.8 \cdot 10^{-4}$	97 % manmade
100 μm	25	90 % manmade
10 μm	328	60 % natural

Consider first the 100 m × 1 cm tape tether. The average area of the tape is 0.5 m^2 and the 3 mm flux is $5.8 \cdot 10^{-4}/m^2$/year. Thus the breaking probability is $5.8 \cdot 10^{-4}$ per year and 0.6 % per 11 years (the maximum duration of the mission, Table 17).

Then let us consider the 5 km long propulsive multi-wire tether which is 8 cm wide. The average area of the tether is 200 m^2 and the 3 cm flux is $1.6 \cdot 10^{-5}$ /m^2/year. Thus the tether's single-blow breaking probability is 0.3 % per year and 3.5 % over 11 years.

The tether can also break due to stochastic breaking of the wire segments it is made of. The wires have 25 μm diameter (EOL) and 20 cm length. The relevant flux is the 10 μm flux which is 328 /m^2/year. The surface area of the wire is $1.57 \cdot 10^{-5}$ m^2 so that the breaking probability is 0.51 % per year year and 5.7 % in 11 years. With five segments, the breaking probability of the tether's unit cell is $0.057^5 = 5.8 \cdot 10^{-7}$ in 11 years. The number of 20 cm long cells in a 5 km long tether is 25000, hence the total breaking probability over 11 years due to stochastic single wire breaking is $25000 \times 5.8 \cdot 10^{-7} = 1.5$ %.

The stochastic breaking probablity increases with the fifth power of mission duration so that if the misson is shorter, the stochastic failure mode is negligible. For example, if one uses two modules, the maximum mission duration is 5.6 years according to Table 17. In this case the single wire segment breaking probability is 2.9 %, the cell breaking probability is $0.029^5 = 2 \cdot 10^{-8}$ and the total tether breaking probability due to stochastic single wire breakings is $25000 \times 2 \cdot 10^{-8} = 0.05$ %, which is almost negligible. The single-blow breaking probability, on the other hand, grows linearly with time.

Thus the total breaking probability of the propulsive tether is 3.5+1.5=5 % over 11 years (longest mission for the single-module system) and 1.9 % over 5.6 years (the longest considered mission for a two-module system), and the breaking probability of the tape tether is 0.6 % per 11 years and 0.3 % per 5.6 years. Thus the single-module system almost but not quite satisfies the max 5 % failure probability requirement over a 11 year mission, remembering that also other components of the system have some nonzero breaking probability.

For heavy satellites and/or high starting altitude, we recommend using two modules for increased performance and higher reliability. In this case the maximum mission length is 5.6 years and the failure probability of the propulsive tether of one of the modules is 1.9 %. If one module's deorbiting capability is lost, the other module still continues at half the original rate. The probability that both modules would fail is roughly $0.019^2 = 0.03$ %, i.e., negligibly small. Thus, adding the second module increases reliability dramatically.

These considerations err on the conservative side in the sense that even if the propulsive tether breaks, the remaining piece of it which is still attached to RU1 continues to be biased at negative voltage by RU1's HV source. The only thing that changes is that

the tether is shorter and it has no endmass so that the gravity gradient force acting on it is much weaker and generally competes head to head with the Coulomb drag. Thus the tether piece in this case goes into significant angle with respect to the vertical which reduces propulsive performance (the amount depends on where the tether was cut). Thus there is a fair chance of deorbiting to succeed even if the tether breaks during deorbiting. The detached RU2 which also has a piece of tether left will deorbit itself quickly because it also carries a redundant HV source. RU2 uses its own body as the electron-gathering surface which reduces the propulsive performance depending on plasma conditions, but still provides a fair amount of thrust. Combined with the low 1.0 kg mass of RU2 the result is fast deorbiting of RU2. Thus, no secondary debris is created even in case of tether breakage.

If the tape tether breaks (the likelihood of which is 0.6 % per 11 years), then the module in question no longer gives any deorbiting thrust to the satellite. The RU1+RU2 combination which is still attached to each other by the propulsive tether deorbits quickly because a piece of the tape tether is still attached to RU1 and provides ample electron collecting area so that the full Coulomb drag gets exerted on the lightweight RU1+RU2 combination. If desired, the tape tether's breaking probability could be lowered by making the tape somewhat wider than 1 cm. However, we think that the present breaking probability is already low enough. Widening the tape would, on the other hand, slightly increase the probability of production of secondary debris, i.e. the risk that the tape would break an impacting space debris object into smaller pieces. The risk that the tape tether would damage an active satellite by direct collision is low, and this probability is practically independent of the tape tether width because the tape width is much less than the size of any active satellite.

As long as it remains in orbit, our to-be-deorbited satellite is tracked and catalogued by ground-based radars so that active satellites can make avoidance manoeuvres when needed. Typically the safe distance used in such manoeuvres is 200 m. Thus, because the tape tether is only 100 m long, such routine avoidance manoeuvres also automatically avoid a collision with the tape tether, not only with our satellite body. The standard avoidance manoeuvres (if the safe distance is 200 m) do not rule out collision with the maintether with an active satellite, but such collision would not damage the active satellite, it only cuts our maintether. The probability of this was calculated above and its consequences for the success of the deorbiting were explained.

Lastly we remark that if many satellites are deorbited by Coulomb drag tethers simultaneously, the risk increases that two Coulomb drag tethers will cross each other. Although the Coulomb drag tether is so thin that it poses no threat to existing space assets, it does present a risk to other Coulomb drag tethers occupying the same orbital volume. Quantitative investigation of this issue is left outside the scope of this study, however, because it is not a near-term concern.

6.2.12.1 Other failure modes besides tether breakage The main failure modes in addition to tether breakage are the following:

F1. Failure of RU1+RU2 separation from the BU.

F2. Main tether deployment failure, either partial or complete, because of motor or its driving electronics or power system failure.

F3. Main tether deployment failure, partial or complete, because of tether getting stuck on the reel.

F4. Failure of RU1 HV subsystem.

For F1, we estimate that the probablity is similar to the failure probability of Cubesat P-POD devices, because they use similar technology. To our knowledge, no P-POD has thus far failed in orbit while 510 cubesats have been launched worldwide (situation January 8, 2017, `http://www.nanosats.eu`). Thus F1 failure probability can be estimated to be insignificant.

For F2, the probability of motor failure is low because relevant space-qualified motors from phySPACE have flown $\sim$ 300 times and also high-value missions such as BepiColombo, Maven, Curiosity rover and Juno have relied on them. Although RU2 where the motor is hosted is a cubesat-sized small environment, it is currently not mass-constrained so that no tradeoffs between mass and reliability are needed in the current design.

For F3, the probablity of this failure mode must be measured experimentally during the development programme by producing several samples of the tether and verifying that they deploy in the laboratory with the same tension force that exists in orbit. In tests performed during the "ESAIL" EU FP7 project, the tether came out correctly from the reel using 0.05 cN tension [11]. The required minimum tension depends on the specific type of the tether (material, wire diameter, number of subwires and production technology).

For F4, there is not yet much flight experience of miniature 1 kV high-voltage sources such as those made by Picoelectronics and EMCO companies. However, the devices are quite lightweight (few grams at minimum) so double or even multiple cold redundancy can be used to improve reliability.

In cases where one uses two plasma brake modules, reliability is very good because of the inherent redundancy. For cases where only one module is installed on the satellite, we think that it will be possible to reach the 95 % reliability goal by specific activities concerning F3 and F4 during the development programme.

6.2.12.2 Risk to active satellites If the maintether collides with an active satellite at orbital hypervelocity, each subwire of the tether makes a small linear scratch where it collides. Satellites survive scratches of same and larger size all the time because of the existing micrometeoroid and debris environment. If the collision is with a solar panel, there could in principle be a risk that exposed conductors of the panel could be short-circuited by the tether (Stephen Taylor, private communication), but because the hypervelocity collision causes the tether to evaporate, such risk does not exist in reality. A concern was also raised during the project that may optical instruments might be harmed by such collisions, but since optical instruments are protected by a baffle, the risk should be minimal (Tiaro Soares, private communication). For example, any baffle-protected remote sensing optical instrument which looks in the direction of Earth is safe, because the orbiting tether piece cannot arrive from within the instrument's field of view. The orbiting tether piece moves in a nearly circular orbit (because the original debris satetellite's orbit typically had low eccentricity, and the eccentricity tends to decrease as the tether piece deorbits by drag processes) and in any case its orbit cannot be such that it would arrive to the satellite from the direction of

the Earth.

Concerning the potential collision risk to active satellites, each plasma brake module comprises one 12.6 μm×1 cm×100 m metallised kapton tape tether, two 1-U cubesat sized remote units and one 8 cm×5 km long tether made of five 35 μm Al 2024 wires.

The cutting probablity of the tether (0.3 % per year) was estimated above using the 3 cm flux. Of course, the active satellite population is only a small subset of the whole $\geq$ 3 cm debris population so that for a given plasma brake tether, the probability that it collides with an active satellite is very small, and even if a collision occurs, it does not harm the active satellite as was discussed in earlier.

The probablity that the tape tether collides with an active satellite is 50 times smaller than for the maintether. In addition, active satellites normally perform avoidance manoeuvres with respect to known objects such as our satellite during deorbiting. The safety distance is normally 200 m. Because the entire tape tether is inside this distance, it means that by actively avoiding the main body, the active satellite also avoids a collision with the tape tether.

Remote Unit 1 is inside the 100 m radius so it is also avoided if the active satellite performs active avoidance. Remote Unit 2 is 5 km from the main body and it can also be avoided if slightly nonstandard avoidance procedure would be used by the active satellite (avoidance of a 5 km long and $\sim \pm 30^\circ$ cone which models the possible orientations of the maintether). With standard 200 m avoidance procedure, Remote Unit 2 forms a statistical threat which is equivalent to a single 1-U cubesat.

In summary, if standard avoidance manoeuvre is used by the active satellite, the risk of harmful collision is equivalent to a single 1-U cubesat (i.e., collision with RU2). By using a larger than standard avoidance manoeuvre it is possible to avoid also this risk.

For those active satellites (e.g., cubesats) that are not able to perform active avoidance, the harmful collision risk is given by the collision risk with the debris satellite itself, the tape tether, RU1 and RU2. Their relative importances depend on the size of the active and the debris satellite, but typically the dominant area risk comes from the tape tether and the debris satellite, RU1 and RU2 posing a relatively smaller risk.

6.2.13 Simulation of tether dynamics

In the ESAIL FP7 project which developed technology for Coulomb drag propulsion in the solar wind (the electric solar wind sail or E-sail for short), general-purpose software "`Vesvision`" was developed for simulating the dynamical behaviour of mechanical systems consisting of rigid bodies and flexible tethers [4, 5]. The core of the simulator is a `C++` library performing high-order accuracy adaptive integration of time-dependent ordinary differential equations (ODEs) and it is callable from `Lua` scripting language using the interface documented in Janhunen [5].

We wrote a `Vesvision Lua` script for simulating dynamics of the plasma brake with parameters listed in Table 19. Forces included in the simulation are the gravity force, the Coulomb drag, the Lorentz force and the force due to thermal contraction and expansion due to temperature changes, especially those related to eclipses. The photon pressure force is not explicitly included because its expected strength is $\sim$100 times lower than Coulomb drag. Neutral atmospheric drag is neglected as well. Its strength is $\sim$ 400 times less than the Coulomb drag.

Table 19: Main input parameters and their code names in `Vesvision Lua` script. Also some informative values e.g. concerning yield and fatigue strength are listed.

Power on during eclipses	`powered_eclipses`	False
Do model tether thermal expansion	`model_CTE`	True
Spacecraft mass	`mspacecraft`	800 kg
Spacecraft side length	`spacecraftsize`	2 m
Initial orbital altitude	`orbalt`	800 km
Orbit MLT sector	`orb_MLTrot`	0° (noon-midnight)
Tape tether length	`tape.L`	100 m
Tape tether width	`tape.w`	1 cm
Tape tether thickness	`tape.h`	12.6 μm
Tape tether Young's modulus	`tape.Young`	3 GPa
Tape tether relative loss modulus	`tape.lossmodulus`	0.06 (polyimide)
(Main)tether length	`tether.L`	5 km
Tether material		Al 2024
Tether Young's modulus	`tether.Young`	73 GPa (Al)
Tether rel. loss modulus	`tether.lossmodulus`	0.02 (Al)
Tether wire radius	`tether.rw`	17.5 μm
Tether wire density	`tether.rho`	2700 kg/m^3
Wire material yield strength		345 MPa
Wire material fatigue limit		138 MPa ($5 \cdot 10^8$ cycles)
Tether wire yield strength (BOL)		33.2 cN
Tether wire yield strength (EOL)		22.8 cN
Tether wire fatigue limit (BOL)		13.3 cN ($5 \cdot 10^8$ cycles)
Tether wire fatigue limit (EOL)		9.1 cN ($5 \cdot 10^8$ cycles)
Tether number of load-bearing wires	`tether.Nparallelwires`	1
Tether number of wires	`tether.Nwires`	5
Tether thermal expansion coefficient	`tether.alphaL`	$2.31 \cdot 10^{-5}$ 1/K
Tether thermal emissivity at 300 K	`tether.epsilon300`	0.04
Tether optical absorptance	`tether.alpha`	0.1
Remote unit height	`ru.length`	10 cm
Remote unit width	`ru.width`	10 cm
RU2 tether attachment point distance	`ru.extralen2`	5 cm
RU1 mass	`mRU1`	0.5 kg
RU2 mass	`mRU2`	1.0 kg
| Tether voltage |	`V0`	1 kV
Earth magn. dipole tilt rel. to orbit	`earth_diptilt`	11°
Mean ion mass	`mi`	$10m_p$
Plasma density	`n0`	$3 \cdot 10^{10}$ m^{-3}
Secondary electron emission coeff.	`chi`	2.0
Coulomb drag per unit tether length	`dFdz`	86 nN/m
Number of tether discr. points	`Np`	30
Timestep	`dt`	0.125 s
Duration of run	`tmax`	10 days

The run predicts the detailed dynamics of the tether and the spacecraft, and the main results are summarised in Table 20 while the data are plotted in Fig. 10. Figure

11 shows a 0.2-day period from the middle of the run which shows more clearly the temporal behaviour in detail.

Table 20: Results of Run 1: the baseline run. Angle variable nomenclature used in side labels of Figs. 10–13 is given in parentheses.

	Mean	Max
Tether tension	1.7 cN	8.9 cN
Loose tether temporal fraction	0.03 %	–
Angle between vertical and satellite–RU2 line (tether vertical angle)	9°	27°
Angle between vertical and satellite–RU1 line (tapetether vertical angle)	15°	64°
Angle between satellite panel normal and tape tether (sat-tapetether angle)	14°	48°
Angle between RU2 roof normal and maintether (RU2–tether angle)	6°	150°

According to the simulation, the tether system swings gently below the satellite with a frequency which is of the order of magnitude of the orbiting period. The maximum swinging angle (the angle between the tether and the vertical direction) over the 10-day simulation period is 27°. By numerical experimentation we determined that the swinging motion is mainly due to the small Lorentz force that acts on the tether as a byproduct of the gathered ion current. The swinging amplitude waxes and wanes between zero and the maximum with about 36 hour period. The reason for this periodicity of the swing envelope function is not known, but we suspect that it is some kind of resonance between the tether's orientation and the Lorentz force.

The baseline run (Run 1) results are most of the time satisfactory, but sometimes the tether becomes loose (tether tension zero) so that RU2 can start to tumble and undergo large-amplitude attitude variations when the tether becomes taut again. This behaviour is due to thermal contraction of the tether when the satellite goes into eclipse. The noon-midnight orbital plane was chosen for the simulation because it corresponds to the worst case regarding how fast the satellite goes in and out from eclipse. Janhunen and Toivanen [7] have analysed the process in the E-sail context. The zero tension events are also associated with adjacent tether tension peaks, although the peak value (8.9 cN) does not exceed any of the material limits, not even the 500 million cycle fatigue limit at EOL. We refer to the original diameter of the wire (35 μm) by BOL, and EOL refers to the wire diameter having been reduced by 6 μm down to 29 μm, corresponding to 5 years of ion sputtering in oxygen-rich plasma under -1 kV negative bias.

The angle between the satellite bottom panel and the tape tether remains moderate (maximum 48°). This is important so that the tape tether does not touch any appendices of the satellite such as its solar panels. Such touching would be risky although not necessarily problematical. The RU2 nearly tips over (maximum angle between its roof panel and the tether is 150°) which is an issue because if the tether rubs against the body of the unit, it might wear down and be eventually cut. The problem can be mitigated by making the RU2 surface smooth.

One can reduce issues caused by tether oscillations by making the equilibrium shape of the load-bearing tether wire somewhat curly. We believe that curling up can be

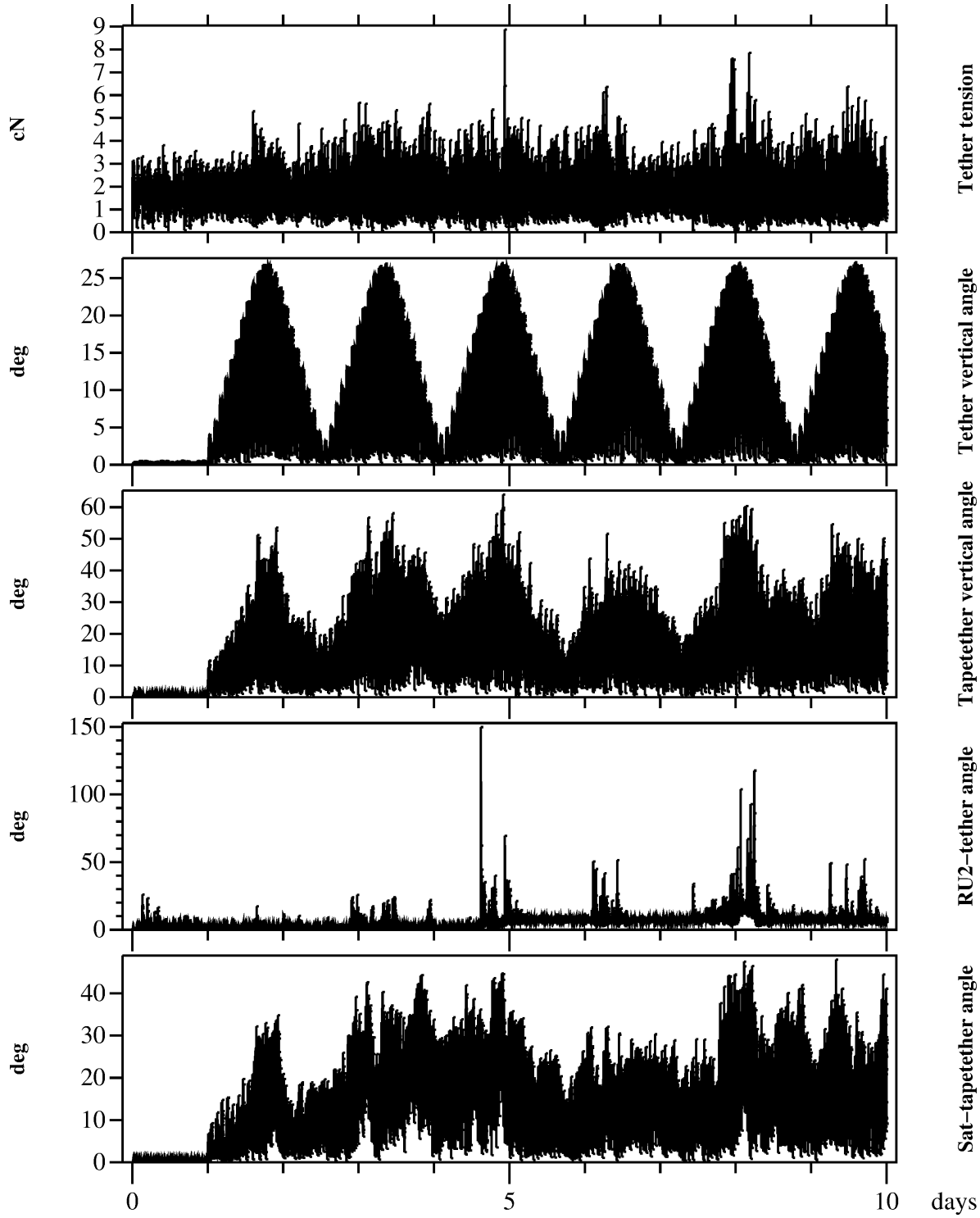

Figure 10: Results of Run 1. For angle variable nomenclature, see Table 20.

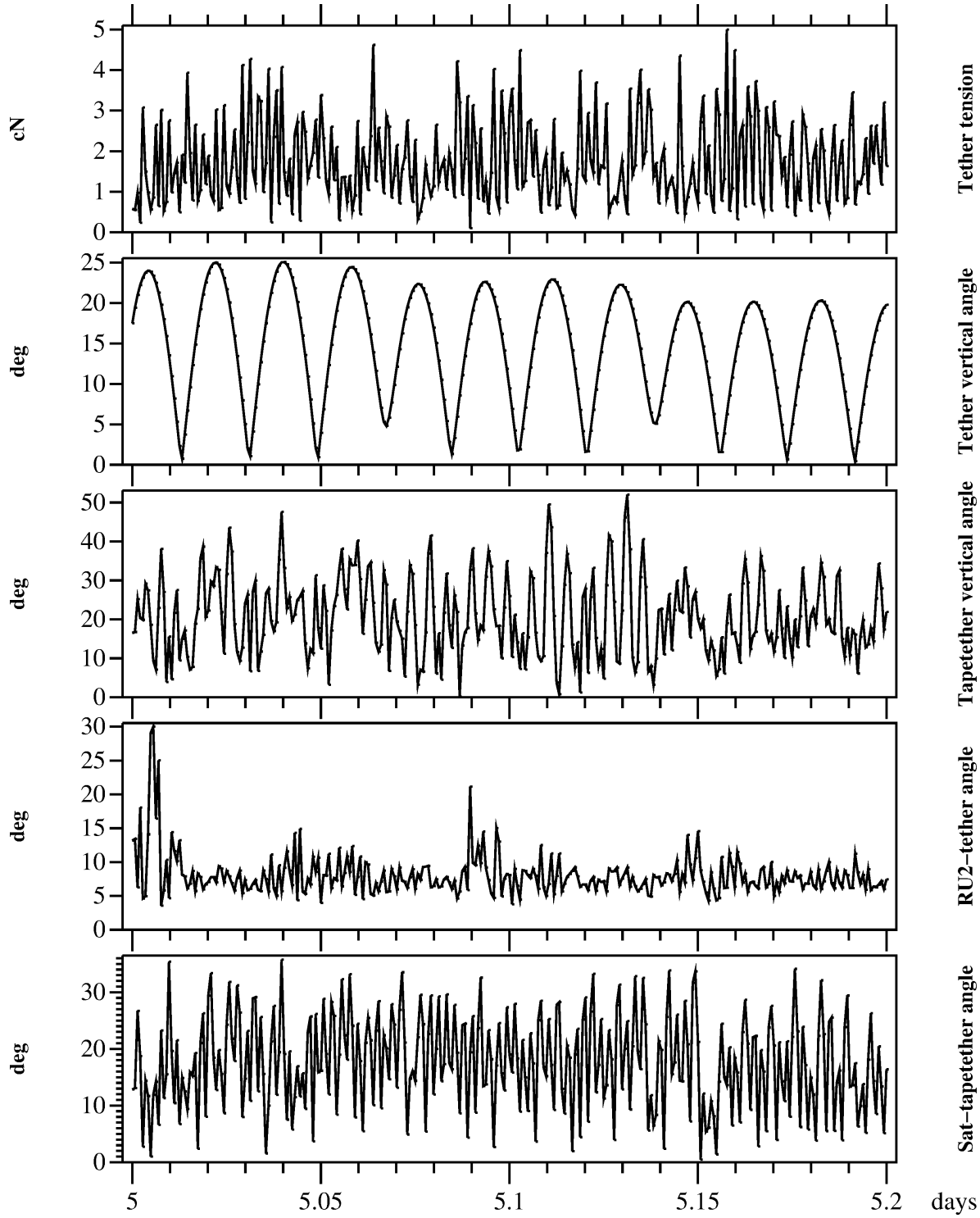

Figure 11: Detail of Run 1 from start of 5th day.

accomplished in a simple way by adding mechanical guides of suitably small radius of curvature in the tether factory. The curled tether needs some minimum tension to straighten up, and the gravity gradient tension at the beginning of deployment is not necessarily enough. To avoid this issue, the part of the tether which is deployed first can be left without curling by removing the guides from the factory at a certain point.

Curling effectively reduces the Young's modulus of the tether and hence decreases the likelihood that the tether becomes loose at any point. To model this, we performed another run (Run 2) which is otherwise identical to Run1, but the tether's Young's modulus is multiplied by factor 0.5. Table 21 summarises the results.

Table 21: Results of Run 2: halved Young's modulus of the tether by wire curling.

	Mean	Max
Tether tension	1.7 cN	6.6 cN
Loose tether temporal fraction	0.007 %	–
Angle between vertical and satellite–RU2 line	9°	27°
Angle between vertical and satellite–RU1 line	13°	46°
Angle between satellite panel normal and tape tether	9°	37°
Angle between RU2 roof normal and maintether	2°	42°

In Run 2, the maximum tether tension is lower (6.6 cN) and the maximum angles between the satellite bottom panel and the tape tether as well as the roof of RU2 and the maintether are lower (37° and 42°, respectively). Some loose tether events still occur, but their duration is apparently short enough that more severe tumbling of RU2 is avoided.

To explore the parameter space further, we perform a third run (Run 3) where the tether's Young's modulus is 0.25 times the original and list the results in Table 22. Now the loose tether fraction is zero and the maximum angle between the RU2 roof normal and the tether has dropped to 8°. In other words, if the Young's modulus of the tether is sufficiently small (25 % of the original), the tether never becomes loose

Table 22: Results of Run 3: Young's modulus of the tether 1/4 of the original.

	Mean	Max
Tether tension	1.7 cN	4.3 cN
Loose tether temporal fraction	0 %	–
Angle between vertical and satellite–RU2 line	9°	27°
Angle between vertical and satellite–RU1 line	12°	45°
Angle between satellite panel normal and tape tether	8°	33°
Angle between RU2 roof normal and maintether	0.7°	8°

To study the effect of ion sputtering which thins the wires, Run 4 (Table 23) is the same as Run 1 except that the wire thickness is 29 μm instead of the original 35 μm which corresponds to the EOL condition after 5-year mission assuming 0.6 μm/a sputtering. The maximum tether tension is now 5.7 cN which is much lower than in the baseline where it was 8.9 cN. The mean and maximum angles are also smaller. Roughly, the EOL result with no wire curling (Run 4) corresponds to the BOL result with wire curled so that Young's modulus is reduced by factor 0.5 (Run 2). Thinning of the

wire by sputtering reduces its spring constant. According to the simulations, reducing the spring constant improves the dynamical behaviour so that the decrease in peak tension(factor 0.64) is even slightly larger than the decrease of the wire's pull strength caused by its reduced diameter (factor 0.69). Here the numbers in parentheses refer to thinning from 35 μm down to 29 μmby sputtering. Hence, BOL simulations (Runs 1, 2 and 3) can be said to represent the worst case situation[5].

Table 23: Results of Run 4: 29 μm tether wires (EOL) instead of 35 μm (BOL).

	Mean	Max
Tether tension	1.7 cN	5.7 cN
Loose tether temporal fraction	0.05 %	–
Angle between vertical and satellite–RU2 line	8°	25°
Angle between vertical and satellite–RU1 line	12°	45°
Angle between satellite panel normal and tape tether	9°	31°
Angle between RU2 roof normal and maintether	3°	69°

Finally, in Figures 12 and 13 we show the data and a temporal detail of Run 4.

Our baseline is to have a battery-free power system. Then illumination changes on the solar panels may affect the tether voltage and therefore the thrust immediately. We made a version of the simulation where the effect was modelled on RU1 by assuming that RU1 is a cube whose six sides are covered by solar panels and estimating the solar panel power based on the actual instantaneous attitude. A change in the unit's attitude changes the available power which changes the tether voltage if the plasma density is high so that the unit is in power-limited regime. Changed tether voltage changes the thrust acting on the tether (both Coulomb drag and Lorentz force), which may cause oscillation of the tether which might again change the attitude of the unit. One might worry that some nonlinear feedback might occur which increases the oscillations. However, in the simulation we did not observe such behaviour. The run where attitude modulation of power was modelled in a worst-case fashion produced nearly identical results with the baseline run.

In conclusion, the simulation predicts that the tether should be able to survive the mechanical loads that occur during the deorbiting mission. That said, it would nevertheless be desirable to try and curl up the load-bearing tether wire so that its effective Young's modulus is reduced, because then loose tether events are absent and consequently the maximum tether tension is lower and also there is no risk that the tether would rub against walls or appendices of the satellite or a remote unit.

[5]Of course, this trend cannot be extrapolated: If sputtering continues for too long (because the wire was initially chosen to be too thin relative to the duration of the deorbiting phase), at some point the wire's fatigue strength would decrease below even the average tether tension which is 1.7 cN in all the runs performed.

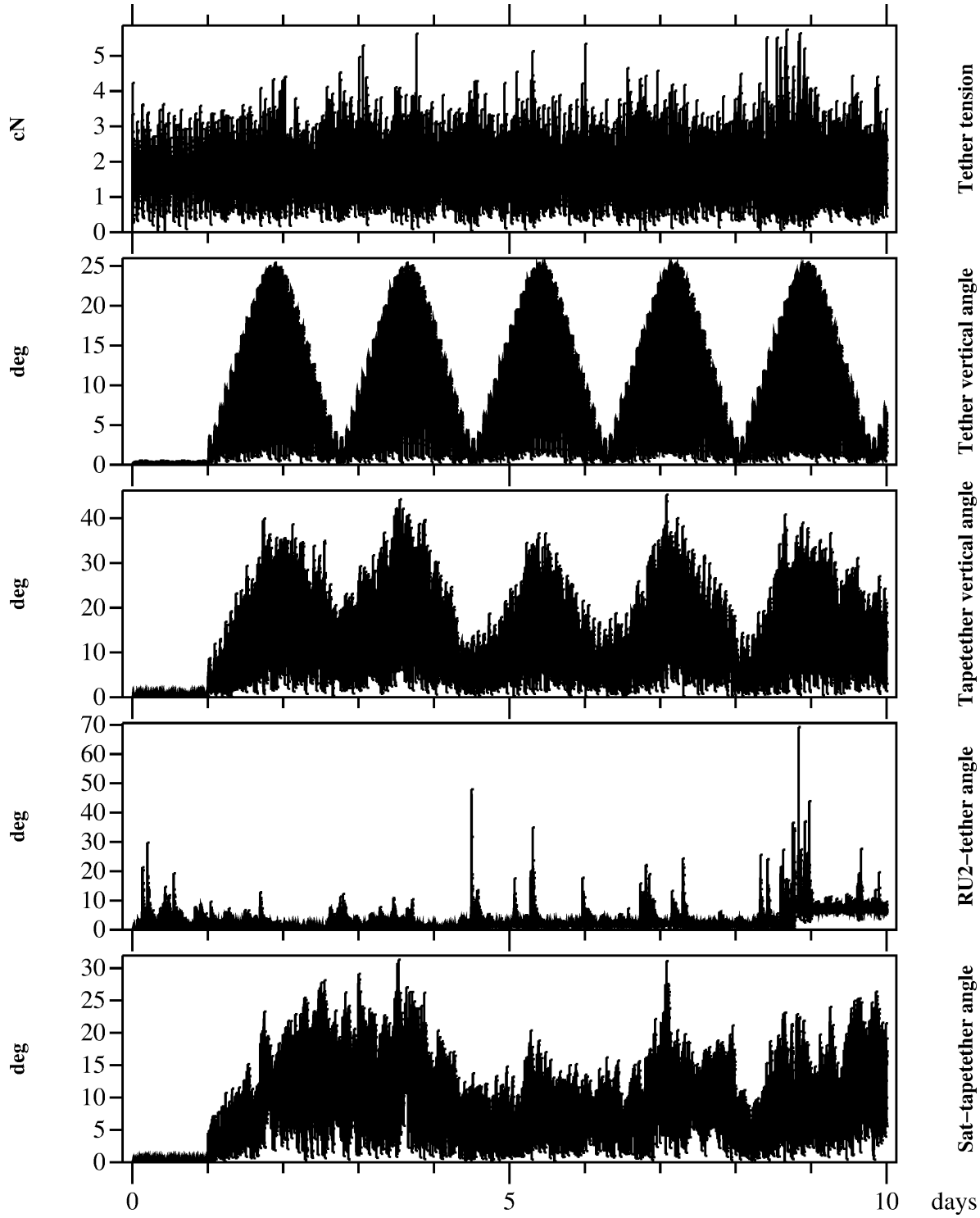

Figure 12: Results of Run 4.

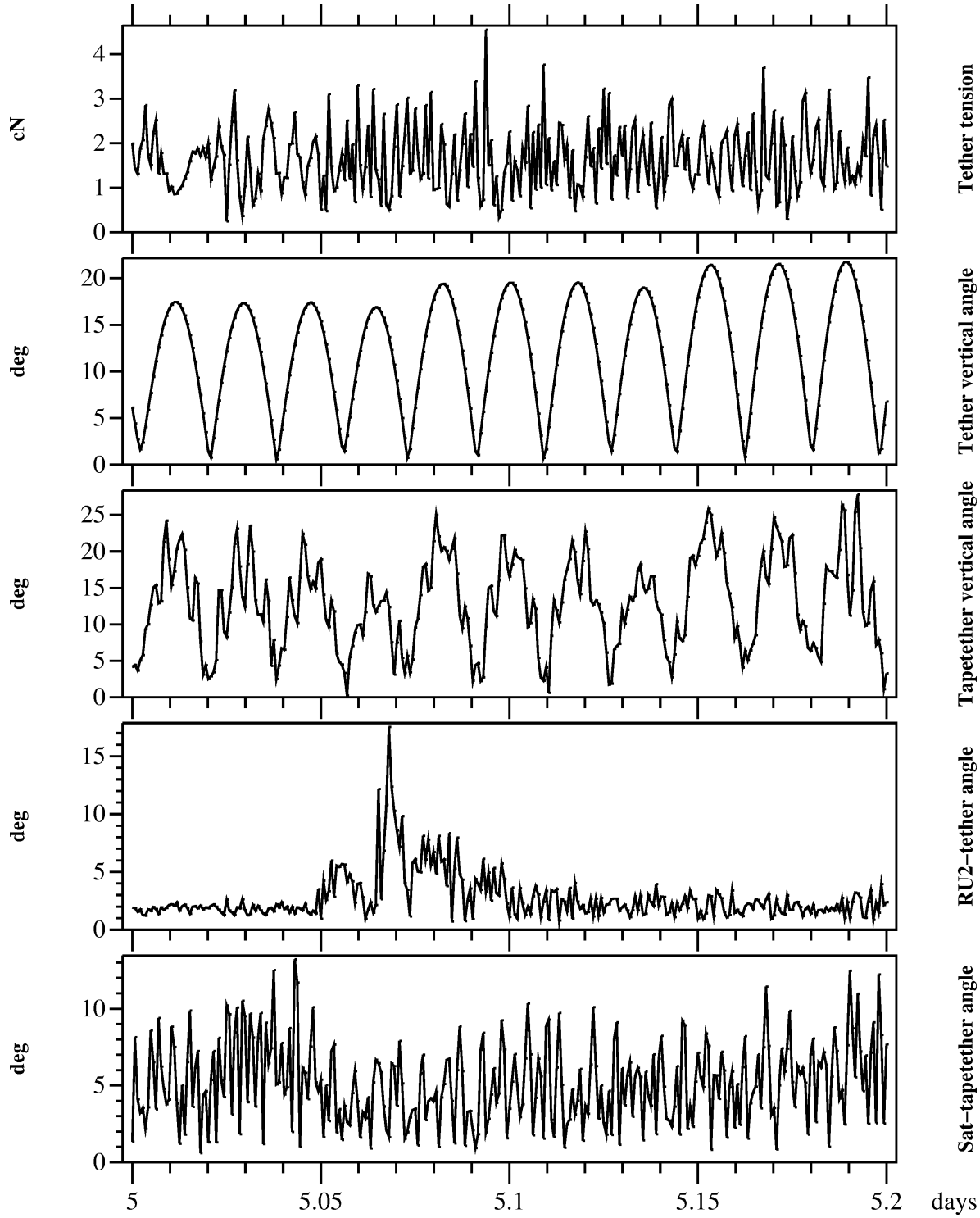

Figure 13: Detail of Run 4 from start of 5th day.

6.2.14 Deployment simulation

We amend the software and methodology described in subsubsection 6.2.13 to perform dynamical simulation of the tape and maintether deployment process. The run starts with downward deployment of the 100-m long tape tether with ejection speed 30 cm/s, so that deployment of the tapetether is complete at about $t = 5.5$ min. Deployment of the 5-km maintether is started at $t = 30$ min with deployment speed 1 cm/s so that maintether deployment is complete after about 6 days.

The results are shown in Fig. 14 and Fig. 15. The panels from top to bottom are: (1) the angle between the satellite bottom panel and the tapetether, (2) the angle between RU1 and the tapetether, (3) the angle between RU2 and the maintether, (4) tension of the tapetether (which is also almost equal to the tension of the maintether).

The satellite's ACS is operative until 2 days from the start. The ACS algorithm used is a simple proportional controller which tries to keep the satellite's bottom panel oriented towards Earth and keep the satellite's spin rate equal to the orbital spin rate. The torque $\mathbf{M}$ applied to the satellite by the ACS is given by

$$\mathbf{M} = \frac{I}{\tau^2} (\hat{n}_\mathrm{b} \times \hat{u}) - \frac{I}{\tau} (\boldsymbol{\omega} - \boldsymbol{\omega}_\mathrm{orb}) \tag{16}$$

where I is the component of the inertial moment of the satellite along the orbital spin axis (i.e. axis perpendicular to the orbital plane), $\hat{n}_\mathrm{b}$ is the normal vector of the satellite's bottom panel, $\hat{u}$ is the local earthward directed unit vector, $\boldsymbol{\omega}_\mathrm{orb}$ is the orbital angular momentum vector and $\tau = 700$ s is a controller timescale parameter. The two terms in Eq. (16) correspond to controls keeping the satellite's bottom panel towards Earth and keeping the spin rate at the desired value, respectively. Although the control terms are mathematically equivalent, we found by numerical experimentation that the presence of both terms is needed for the controller to work well. Operating the ACS during the tape tether deployment and during early stages of the maintether deploymet is mandatory because otherwise the satellite's orientation would not be dynamically stable, according to our simulations. The system is passively stable, however, when the maintether is long enough so that the gravity gradient force is sufficiently large, so that after 2 days, at least, it is safe to turn the ACS off and to passivate the satellite.

The conclusions for dynamical features of deployment are strictly valid only for the particular case simulated, i.e. a 800 kg and 2 m cubical satellite at 800 km polar noon-midnight orbit. A more complete investigation would require simulating also other values of satellite mass and inertial moment tensor, but is outside the scope of the present study. We expect, however, that deployment can be made to work also with smaller satellites, either directly or perhaps by adjusting the timescale parameter τ of the deployment-time ACS controller.

We also made a deployment run where a tether system is quasi-simultaneously deployed both downward and upward from the satellite. A small difference in tape ejection speed was introduced – likely to occur also in reality – so that the tapes tighten at a bit different times. The results are show in Fig. 16. The quantities shown related to the lower tether, but the upper tether quantities are similar. The system is slightly more restless than the single-tether system, but the difference is not large. The maximum angle between RU2 roof and the tether is about 80°. This is rather close to 90° at which point the tether would touch the roof of RU2 which might – if it would occur repeatedly – eventually be a risk to the tether's integrity.

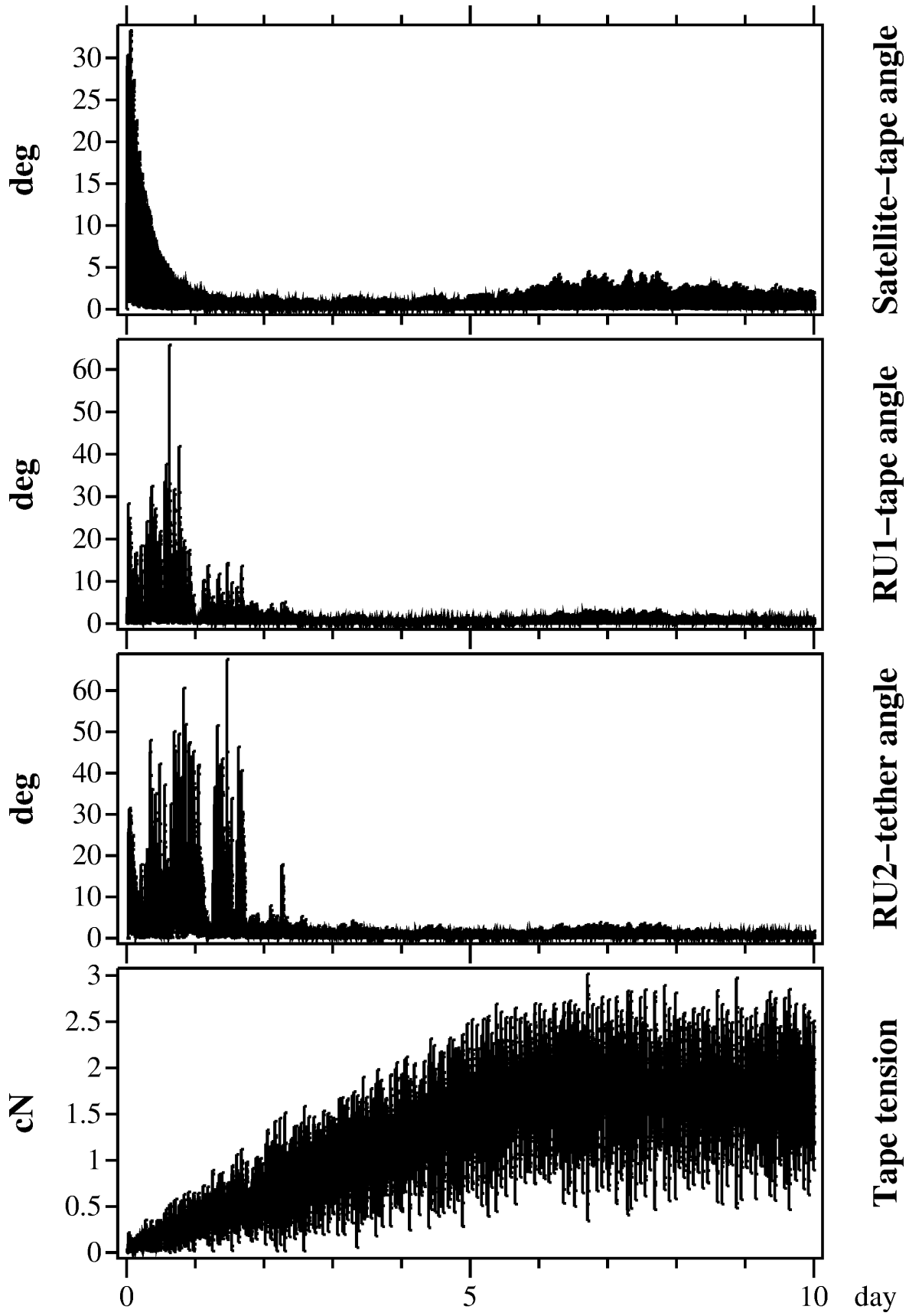

Figure 14: Results of deployment dynamical simulation run with single (downward-deploying) tether system.

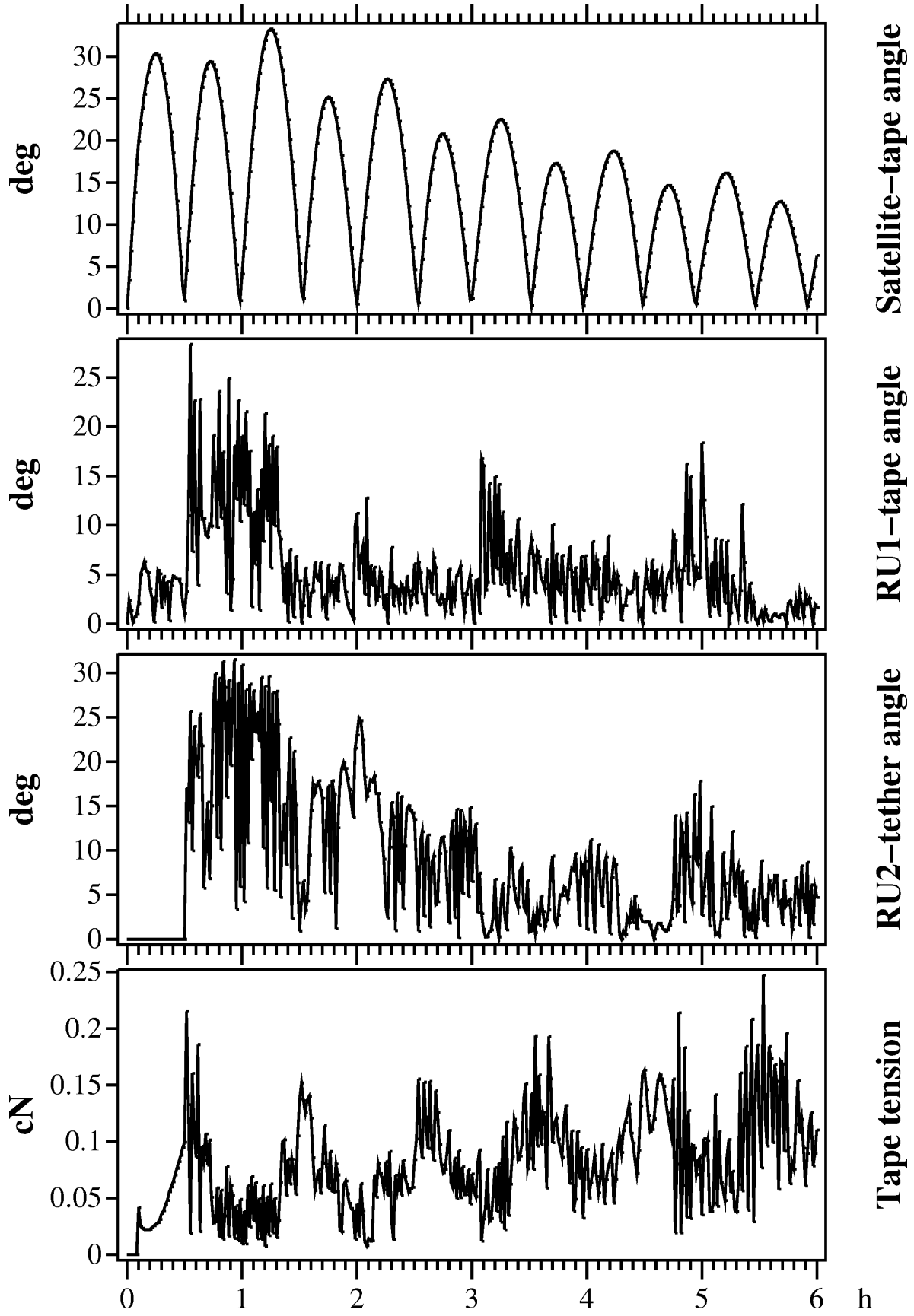

Figure 15: The first six hours of Fig. 14.

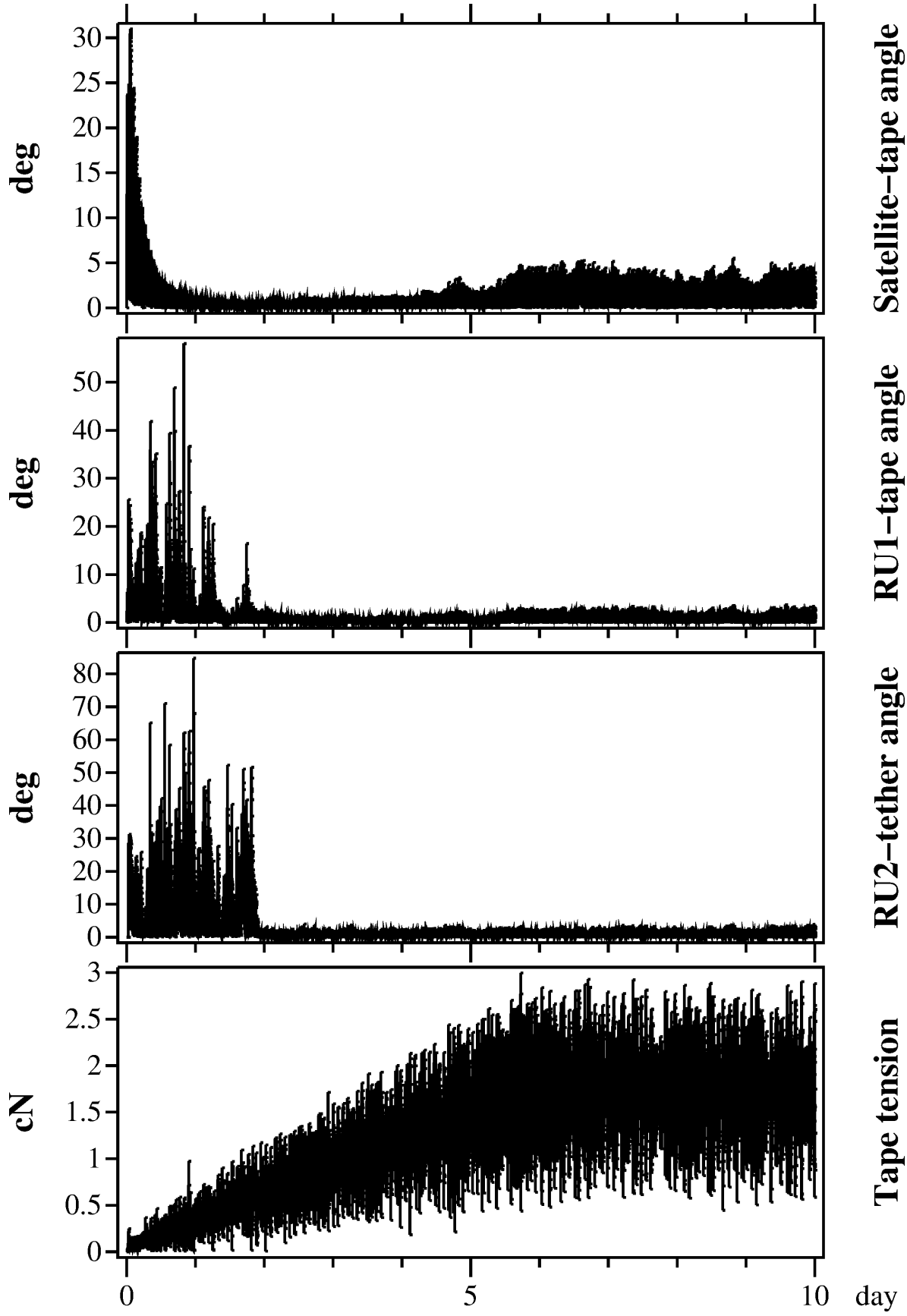

Figure 16: Deployment simulation for two-tether system.

7 Development plan

Notice: this section (7) does not appear in the public web version of the document.

7.1 Development roadmap

7.1.1 Foreseen activities

Table 24 lists activities needed to reach TRL 7.

Table 24: Development activities foreseen to reach the given TRL.

	Activity	Target	k€
WP1	Development of generic low-cost tether manufacturing technology which can be applied to at least aluminium or nickel and preferably other metals.	TRL 3	200
WP2	Prototyping of tape tether and its opening mechanism (spring, brake, study of tape perforation option).	TRL 3	30
WP3	Production of several sample tethers and demonstration that they deploy correctly.	TRL 4	150
WP4	Build TRL 5 plasma brake module model and perform standard TRL 5 environmental testing for it.	TRL 5	300
	Total to reach TRL 5		*680*
WP5	Option A: Test mission where plasma brake module is deployed from a satellite, operated for a while and then released while continuing to deorbit itself. Option B: Self-contained 3-U cubesat test mission where 2-U part is the plasma brake module and 1-U part is the satellite.	TRL 7	2000 600
	Total to reach TRL 7: *Option A* *Option B*		*2680* *1280*

In Option A of WP 5, our baseline idea is that after deployment from the satellite, the plasma brake device is jettisoned relatively quickly so that the satellite can continue its other operations or scientific experiments. After jettisoning the plasma brake module continues to operate and therefore deorbits itself quickly. The benefit of this arrangement is that the experiment can be hosted on almost any LEO satellite (the only requirement is a functioning ACS), performing it does not take a long time so that it places no burden on other parts of the satellite's mission, and it can be done in an early phase of the mission so that we get the results quickly. Naturally, *if* there would be a satellite mission which for any reason needs to lower its orbit in an early mission phase, combining the plasma brake test with it would produce additional benefits for both parties.

In Option B of WP 5, we launch a 3-U cubesat using normal cubesat launch procedures. One unit of the cubesat acts as the satellite to be deorbited and the other two units form the plasma brake module which is identical to the module to be used in larger satellites. The 1-U satellite needs basic facilities of a cubesat: power system, communication system and ACS.

In addition to these options, we remark that the Aalto-1 satellite (3-U cubesat) is scheduled for launch in Q1/2017 and it carries a 100 m long aluminium tether made by

the ultrasonic bonding technique. Additionally, the ESTCube-2 satellite project (also a 3-U cubesat) is offering to us a flight testing opportunity for a new type of tether which we can hopefully use, depending on available funding.

7.1.2 Initial TRL

The TRL of a plasma brake module was 1 before this project. The TRL of aluminium tether for Coulomb drag utilisation was 4, and the TRL of gold tether was 3. The TRL of a short tether spin deployed Coulomb drag cubesat experiment is 5-6 (experiment integrated into Aalto-1 cubesat which is waiting for launch).

7.1.3 Final TRL

The TRL of a plasma brake module increased from 1 to 2-3 during this project (September-November 2016). The other TRL's did not change.

7.2 Identification of risks

The main technical risk is in developing the tether manufacturing methods. For aluminium tethers (Al99Si1 alloy) we already have a TRL 4 production method; however, the method is somewhat inherently expensive and cumbersome to maintain. For gold, we have a TRL 3 method which is more robust, but again, increasing the TRL always carries some risks. For other metals, we have TRL 1 ideas for generic production which we believe are viable, but starting from a low TRL always carries some risk.

However, the fact that we have several options available for tether manufacture decreases the overall risk, provided that adequate non-recurrent R&D resources are available.

When discussing tether manufacturing methods, one requirement is that the tether tension needed in the deployment phase is low enough so that the spring-deployment concept is viable. If this condition is not fulfilled for the chosen tether type and deployment method, then we could run into trouble with the spring-assisted concept. The problem could be mitigated by increase the mass of the RU2 and/or by increasing the length of the tape tether from the default 100 m. The latter alternative should then be traded against the increased risk of producing secondary debris. However, we are rather confident that this problem will not arise or that if it arises, it can be treated by pulling the tether out from the reel by a capstan mechanism.

7.3 Assembly, integration and test

Assembly and integration of the unit itself is not difficult because the functions are mainly only mechanical and because the design is not mass or volume constrained. For what concerns the tether, it is likely advantageous to produce it directly onto the flight model reel, which implies some constraints on scheduling and logistics. Quality control by destructive testing can be applied to pieces of tether produced by the factory before and after producing the flight-model tether.

Testing the unit involves testing its mechanical functions. Some mechanical functions are one-off devices such as spring-powered launch locks which cannot be tested after arming them.

7.4 Costs

For R&D cost estimates to reach TRL 5 and TRL 7, see Table 24.

For the recurrent cost[6], we estimate 48 k€ per module. The cost breakdown is given in Table 25.

Table 25: Recurrent cost of single plasma brake module.

Mechanical parts for BU, RU1, RU2	10 k€
Solar panels for RU1 and RU2	15 k€
Power system and other electronics	5 k€
Motor for RU2	8 k€
Maintether	10 k€
Total	48 k€

8 Conclusions

1. Satisfying the requirements is possible: we can deorbit up to 800 kg/850 km or 200 kg/1200 km orbit satellites using a device whose single module weighs 2 kg and uses 2-U volume. For larger satellites we however recommend two modules (one deploying tether upward and the other downward) for higher performance and extra reliability. A single-module system can almost but not quite satisfy the 95 % reliability requirement for the 800 kg/850 km class, but using two modules improves the reliability and speeds up deorbiting.

2. Leaving tether manufacture technology aside, the devices are simple and low-cost and the amount of digital electronics needed is minimal.

3. The devices are benign to other space assets and the Remote Units deorbit themselves quickly in case of tether breakage. It is also easy to add a second HV source to enhance reliability of deorbiting.

4. *(Notice: this item does not appear in the public web version of the document.)* Further R&D is motivated to select the best tether material and to develop manufacturing technology for it. Currently the materials that would suit best for this purpose (aluminium, nickel) do not have a low-cost high TRL tether manufacturing method and vice versa. We recommend selecting a good material (aluminium and/or nickel) and developing a scalable manufacturing technology for it, rather than using a material (gold) which has issues although it can satisfy the requirements on paper.

[6] Assuming one makes 100 units in total.

A Annex 1: Facilities and tools used for the study

A.1 Code used for calculating deorbit times in Table 17

Listing 1: `deorbit.t Tela` (`http://space.fmi.fi/prog/tela.html`) program.

```
mp = 1.67e-27;
e = 1.602e-19;
epsilon0 = 8.85e-12;
R_E = 6371.2e3;
GM_E = 3.986583366e14;
// ------------------------------------------------
m = 400.0;              // satellite mass (kg)
L = 5e3;                // tether length (m)
Ntethers = 2;           // number of tethers (1 or 2)
rw = 10e-6;             // tether wire radius (m)
Nw = 5;                 // number of wires in tether
ballistic = 130.0;      // ballistic coefficient of the satellite (kg/m^2)
initalt = 850e3;        // initial altitude (m)
turnoffalt = 0*570e3;    // altitude where Coulomb drag turned off (m)
chi = 2.0;              // secondary electron coefficient
// ------------------------------------------------
maxorbits = 200000;
r = R_E + initalt;
t = 0.0;
u = import1("msis.dat");
msis_alt = u[:,1]*1e3;
msis_rho = u[:,2];
//msg_given = 0;
sputter_fluence = 0.0;  // accelerated oxygen ions per m^2
//V0s = zeros(maxorbits); alts=V0s; FCs=V0s; ts=V0s;
for (j=1; j<=maxorbits; j++) {
    v = sqrt(GM_E/r);
    tau = 2*pi*r/v;
    F = NeutralDrag(r,v);
    if (r-R_E > turnoffalt) {
        [FC,V0,Oionflux] = CoulombDragThrust(r,v);
        sputter_fluence+= Oionflux*tau;
        F+= FC;
    };
//  FCs[j] = FC;
//  V0s[j] = V0;
//  alts[j] = r-R_E;
//  ts[j] = t;
//  F =  FC + FN;
//  if (FN > FC && !msg_given) {
//      format("Neutral drag starts to dominate from `` km, t=`` a\n",
//             (r-R_E)*1e-3,t/(24*3600*365.25));
//      msg_given=1;
//  };
    a = F/m;
    deltav = a*tau;
    v+= deltav;
    r = GM_E/v^2;
    if (r < R_E+200e3) break;
    t+= tau;
```

```
};
/*
FCs = FCs[1:j]; V0s = V0s[1:j]; alts = alts[1:j]; ts=ts[1:j];
plot(alts*1e-3,V0s,"xlabel","km","ylabel","V","toplabel","Voltage versus
    altitude","ymin",0);
plot(alts*1e-3,1e9*FCs/(Ntethers*L),"xlabel","km","ylabel","nN/m","
    toplabel","Coulomb drag","ymin",0);
plot(ts/(24*3600*365.25),alts*1e-3,"xlabel","a","ylabel","km","toplabel
    ","Altitude versus time");
*/
format("Deorbiting time: `` years\n",t/(24*3600*365.25));
format("Sputter erosion/Au: `` um\n",1e6*sputter_fluence*1.08*197*mp
    /19300);
format("Sputter erosion/Cu: `` um\n",1e6*sputter_fluence*1.477*63.5*mp
    /8900);
format("Sputter erosion/Ni: `` um\n",1e6*sputter_fluence*0.894*58.7*mp
    /8900);
format("Sputter erosion/Ta: `` um\n",1e6*sputter_fluence*0.276*181*mp
    /16700);

// ------------------------------------------------------

function [n,mi] = PlasmaProperties(alt)
global(mp)
{
    altvec = #(600e3, 800e3, 1000e3,1200e3);
    mivec =  #(14.9,  10.7,  6.7,    5.4);
    nvec =   #(1.5e11,5.3e10,2.6e10,1.5e10);
    alt1 = limit(alt,600e3,1200e3);
    n = interp(altvec,nvec,alt1);
    mi = interp(altvec,mivec,alt1)*mp;
};

function [F,V0,Oionflux] = CoulombDragThrust(r,v)
global(R_E,e,epsilon0,L,Ntethers,rw,Nw,chi,mp)
{
    // ----------------
    V0max = 1e3;
    P = 1.5; // power per device (W) (if Ntethers=2, total pwr is 2*P)
    // ----------------
    rwstar = sqrt(rw*0.1);
    [n0,mi] = PlasmaProperties(r-R_E);
    // P=chi*e*n0*sqrt(2*e/mi)*2*rw*Nw*L*V0^(3/2)
    V0 = min(V0max,(P/(chi*e*n0*sqrt(2*e/mi)*2*rw*Nw*L))^(2/3));
    // mi = 1-fO + 16*fO = 1+15*fO, fO=(mi-1)/15
    nOxy = n0*(mi/mp-1)/15;
    Oionflux = nOxy*sqrt(2*e*V0/(16*mp))/pi;
    Oionflux*= sqrt(V0/1e3); // sputter yield approximately ~energy^0.5
    Pdyn = mi*n0*v^2;
    lambdaDeff = sqrt(epsilon0*V0/(e*n0));
    Vtilde = V0/log(lambdaDeff/rwstar);
    Vi = 0.5*mi*v^2/e;
    dFdz =
    (1-0.5*0.27)*3.864*Pdyn*sqrt(epsilon0*Vtilde/(e*n0))*exp(-Vi/Vtilde);
    F = Ntethers*L*dFdz;
};
```

```
function F = NeutralDrag(r,v)
global(msis_alt,msis_rho,R_E,ballistic,m,L,Ntethers,rw,Nw)
{
    // ----------------------
    area_tapetether = 0.5; // mean ram-facing area of tape tether
    // ----------------------
    rho = interp(msis_alt,msis_rho,r-R_E);
    A = m/ballistic;
    A+= Ntethers*area_tapetether + Ntethers*L*Nw*rw;
    F = rho*v^2*A;
};
```